Nanoscale Advances

ROYAL SOCIETY OF CHEMISTRY

REVIEW

View Article Online
View Journal | View Issue

Cite this: *Nanoscale Adv.*, 2025, **7**, 3160

Bimetallic nanoparticles as pioneering eco-friendly catalysts for remediation of pharmaceuticals and personal care products (PPCPs)

Jyoti Rani,[a] Tamanna Goyal,[a] Arshdeep Kaur,[a] Subbulakshmi Ganesan,[c] Ashwani Kumar Sharma,[d] Ashish Singh Chauhan,[e] Sandeep Kaushal *[b] and Sandeep Kumar *[a]

Received 14th February 2025
Accepted 10th April 2025

DOI: 10.1039/d5na00151j

rsc.li/nanoscale-advances

The persistent presence of Pharmaceuticals and Personal Care Products (PPCPs) in aquatic environments poses a significant risk to both human health and ecosystems, with conventional water treatment methods often unable to effectively remove these contaminants. Recent research has identified bimetallic nanoparticles as a promising and eco-friendly solution for PPCP remediation, owing to their enhanced catalytic properties and the synergistic effects between the metals. This review critically examines the synthesis, characterization, and application of bimetallic nanoparticles for the degradation of PPCPs in water. Key synthetic approaches, particularly green synthesis methods, are explored,

[a]*Department of Chemistry, Akal University, Talwandi Sabo, Bathinda-151302, Punjab, India. E-mail: sandeepchem83@gmail.com*

[b]*Regional Institute of Education, National Council of Educational Research and Training, Ajmer, Rajasthan, India. E-mail: kaushalsandeep33@gmail.com*

[c]*Department of Chemistry and Biochemistry, School of Sciences, JAIN (Deemed to be University), Bangalore, Karnataka, India*

[d]*Department of Applied Sciences, Chandigarh Engineering College, Chandigarh Group of Colleges, Jhanjeri, Mohali 140307, Punjab, India*

[e]*Uttaranchal Institute of Pharmaceutical Sciences, Division of Research and Innovation, Uttaranchal University, Dehradun, Uttarakhand, India*

Jyoti Rani

Jyoti Rani graduated from Mata Harki Devi College for Women, Odhan. She holds a post-graduate degree in Chemistry from Akal University, Talwandi Sabo and is currently pursuing a PhD under the supervision of Dr Sandeep Kumar, Assistant Professor, Department of Chemistry at Akal University, Talwandi Sabo, Punjab, India. Her area of interest is materials science and environmental remediation.

Sandeep Kaushal

Dr Sandeep Kaushal is a distinguished materials scientist and Associate Professor at the Regional Institute of Education (RIE), NCERT, Ajmer, India. With over 80 research publications in high-impact international journals, Dr Kaushal has established himself as a leading expert in materials science, photocatalysis, nanotechnology, and environmental remediation. His innovative work has also led to two patents, showcasing his commitment to translating research into impactful solutions. In 2021, he was recognized as Top Cited Author by the Royal Society of Chemistry (RSC), further solidifying his influence in the scientific community. He serves as a reviewer for several prestigious journals, such as Chemical Engineering Journal, Journal of Environmental Engineering Chemistry, Materials Today Chemistry, Energy & Fuels, Journal of Materials Chemistry A, ACS Applied Energy Materials, journal of the Taiwan Institute of Chemical Engineers, and Solar Energy. His active participation as a reviewer reflects his dedication to maintaining the highest standards of scientific research.

emphasizing their ability to control nanoparticle morphology, size, and composition. We highlight the novel catalytic mechanisms employed by bimetallic nanoparticles, including electron transfer, surface reactions, and adsorption processes, which contribute to efficient PPCP removal. Furthermore, the influence of critical factors such as nanoparticle size, composition, and surface functionalization on catalytic efficiency is analyzed. Key findings include the superior performance of bimetallic nanoparticles over monometallic counterparts, with specific emphasis on their ability to degrade a wide range of PPCPs under mild conditions. However, challenges such as scalability, stability, and environmental impact remain. This review also provides insights into the future directions for bimetallic nanoparticle development, stressing the importance of interdisciplinary research and collaborative efforts to optimize their design for large-scale, sustainable water treatment applications. Overall, this work offers a comprehensive understanding of how bimetallic nanoparticles can be optimized for sustainable water treatment solutions, highlighting their potential to mitigate the adverse effects of PPCPs on both ecosystems and public health.

1. Introduction

Pharmaceuticals and Personal Care Products (PPCPs) consist of a wide range of substances, including medications such as antibiotics (penicillin, sulfonamide, macrolides, fluoroquinolones, protein synthesis inhibitors), hormones (endocrine disruptor hormones like estrone, estriol, estrogens, 17-β-estradiol, testosterone, 17-α-ethinylestradiol), analgesic and anti-inflammatory drugs (common prescribed are ibuprofen, naproxen, acetaminophen, and diclofenac), antiepileptic drugs (carbamazepine), β-blockers (for cardiac dysfunctions like sotalol, atenolol, theophylline, metoprolol, salbutamol), blood lipid regulators (commonly known as statins), contrast media, and cytostatic drugs (cancer therapeutics), *etc.*[1] Other pharmaceuticals may include preservatives, disinfectants, synthetic musk (used in antiseptics and surface disinfection), antimicrobial agents (fungicides), sunscreen creams (UV filters), *etc.*[2]

Personal care products can be broadly categorized into the following groups: cosmetics, skincare (UV filters for sunscreen) and hair care products, synthetic fragrances (used in perfume and deodorants, essence, body lotion, shower and bath products, skin or hair care products), pesticides and insect repellent, preservatives (used in medical devices, packaging textiles, functional clothing, and household items), and other personal care items.[3] PPCPs can enter the environment through various pathways, such as domestic wastewater discharges, improper disposal of effluents and solid waste from clinical laboratories and hospitals, excretion by humans and animals, biosolids for agricultural applications, and urban landfills including dumping of unused cosmetic or medicinal products.[4] Besides this, the major contributor of PPCPs to the environment is the sewage and wastewater treatment plants (WWTPs).[5] The sewage and water treatment effluents contain various classes of PPCPs: anti-inflammatory drugs, antibiotics, hormones (endocrine mimicking substances), β-blockers, lipid regulators, *etc.*[6] Once in the environment, these substances can accumulate in soil, water bodies, and sediments. Many PPCPs even at low concentrations are toxic to aquatic organisms, such as fish, algae, and invertebrates. These can disrupt aquatic ecosystems and harm biodiversity.[7] Within the pharmaceutical category, antibiotics have gained significant attention of the scientific community due to their extensive usage in both human medicine and livestock farming. The prolonged exposure to antibiotics may lead to the development of resistant strains of bacteria, raising concerns for public health.[8] Further, certain chemicals found in personal care products, such as phthalates and parabens, have been linked to endocrine disruption in wildlife and humans.[9] These substances can interfere with hormonal systems and reproductive functions.[10] Certain PPCPs have the potential to accumulate in the tissues of organisms through bioaccumulation and biomagnification along the food chain.[11] This can lead to higher concentrations of contaminants in apex predators, posing risks to their health and survival. This risk is linked to changes in the behavior, physiology, and reproductive success of wildlife, including alterations in hormone levels, mating behavior, and developmental patterns.[12]

To tackle the environmental repercussions of PPCPs, a comprehensive approach is required including enhanced regulatory measures, advanced wastewater treatment methods, adoption of appropriate disposal protocols, and the promotion of eco-friendly alternatives in pharmaceuticals and personal

Sandeep Kumar

Dr Sandeep Kumar is an Assistant Professor in the Department of Chemistry at Akal University, Talwandi Sabo, Punjab, India. He completed his MSc and PhD in Chemistry at Guru Nanak Dev University, Amritsar, where he focused on developing optical sensors for detecting anions in aqueous solutions. His current research interests center on the surface modification of waste biomass materials through nanostructuring for environmental remediation. This includes the removal of organic and inorganic contaminants from water using techniques like advanced oxidation processes (AOPs). His work contributes to the development of efficient, sustainable methods for wastewater treatment and environmental cleanup, with an emphasis on optimizing AOPs for various contaminants.

Table 1 Comprehensive summary of review papers from the literature based on bimetallic nanoparticles and their applications (since 2020 onwards)

Focus of review	Synthetic approach	Application	Ref.
Bimetallic nanoparticles of noble metal like Pt, Ag and Au were focused for their structural features and macroscopic properties like light absorption, antibacterial effects, and catalytic activity	Chemical method	Heterogeneous catalysis and biomedical applications	26
The review provides information on synthetic approaches for bare and supported bimetallic nanoparticles with focus on the relation between synthesis routes, properties, and resulting efficiencies	Chemical method	Biomedical application	27
The review focus on the synthetic strategies of bimetallic nanoparticle/metal–organic framework (NP/MOF) composites and their activities for various heterogenous catalysis	Chemical methods	Co oxidation, heterogeneous catalysis	28
The review presents bimetallic nanoparticles as anticancer, drug delivery, and imaging agents	Physicochemical approaches and green synthesis	Biomedical application	29
The review is based on semiconductor/bimetallic nanoparticles-based composites for enhanced photo-redox catalysis	Chemical methods	Photocatalytic environmental remediation	30
The review focus on the structure–reactivity relationships in heterogeneous bimetallic catalyst	Chemical methods	Heterogenous catalysis	31
The review is focused on synergistic mechanism of bimetallic nanoparticles/polymeric carbon nitride (PCN) composites for redox catalysis, electrocatalysis, and photocatalysis	Physical and chemical methods	Redox catalysis, electrocatalysis, and photocatalysis	32
The review is based on supported bimetallic nanoparticles (BMNPs) for direct methanol fuel cell (DMFC)	Chemical methods	Methanol oxidation in direct methanol fuel cells	33
The review discussed the bimetallic nanoparticles (BMNPs) as antimicrobial resistance (AMR)		Biomedical applications	34
Focuses on the antibacterial activity and mechanisms of action bimetallic nanoparticles	Biological methods	Biomedical applications resistance	35
The review focus on development of bimetallic nanomaterials and their nanocomposites for enhancing biosensor capabilities	Conventional methods, electrodeposition, and green approach	Biosensing applications	36
The review is based on the bimetallic nanoparticle's size, structure, and morphology relationship to address the environment remediation challenges	Physical, chemical, and biological synthesis	Environmental remediation applications	37
The review focus on bimetallic nanoparticle-based electrochemical sensors for biomolecule detection	Physical and chemical methods	Biosensing applications	38
Focuses on the antibacterial activity and mechanisms of action bimetallic nanoparticles	Physical, chemical, and biological synthesis	Biomedical applications	39
Bimetallic nanoparticle-graphene oxide and bimetallic nanoparticle-metal organic framework nanocomposites as potential catalysts for hydrogen evolution reaction (HER)	Chemical methods	Hydrogen production and storage	40
Bimetallic CuFe (copper-iron) nanoparticles and its composites as catalysts	Physical and chemical methods	Electrocatalysis, photocatalysis, and other catalytic reactions	41
Bimetallic nanoparticles were used for waste water treatment and antimicrobial agents	Physical and chemical methods	Antimicrobial activities, and wastewater treatment	25
Focus on the different physicochemical properties of bimetallic nanoparticles than those of monometallic nanoparticles. Treatment of organic and inorganic pollutants in water and wastewater using bimetallic nanoparticles	Physical, chemical and biological methods	Removal of organic (dyes, phenols and chlorinated organic compounds) and inorganic pollutants (nitrate and hexavalent chromium)	42
The review focus on dominance of chemical methods as high-yield approach for BNP synthesis and application of bimetallic nanoparticles in water treatment, breath sensing, catalysis and hydrogen storage	Physical, chemical and biological methods	Water treatment, biomedical uses, breath sensing, and hydrogen storage	43
A short review with main focus on the synthesis methods with a brief discussion on biological and environmental remediation	Physical, chemical and biological methods	Application in fields including medicine, agriculture, water treatment, nanotechnology, and catalysis	44
The review focus on the advances in synthetic techniques for bimetallic oxides, choice of metal combination, and mechanistic description for interaction with various pollutants	Physical, chemical and biological methods	Wastewater treatment (removal of organic contaminants)	45

Table 1 (*Contd.*)

Focus of review	Synthetic approach	Application	Ref.
Iron-based bimetallic nanoparticles were discussed for water remediation through heterogeneous advanced oxidation processes	Physical, chemical and biological	Activation of peroxygens for degradation of organic and inorganic contaminants	46
The review focus on the adsorption efficiencies and synergy between bimetallic nanoparticles and various substrates used for making nanocomposites for water remediation	Physical and chemical methods	Removal of multiple contaminants from water and wastewater using synergies between substrates and metal ions	47
The review emphasizes on the bimetallic nanoparticle substances as tools to attain sustainable development goals (SDG 3, SDG 6, and SDG 12 *i.e.* good health and well-being, clean water and sanitation, and responsible consumption and production, respectively)	Green synthesis	Bimetallic nanoparticles as sustainable material offering potential solutions for environmental remediation, and improving health	48
The review focus on exploring the role of bacteria, fungi, yeast, and algae in producing metal nanoparticles with environmental applications	Biological methods	Environmental remediation applications	49
The review focus on green route synthesis of Au/Ag bimetallic nanoparticles with potential applications in various fields, including biosensing, imaging, nanomedicine, catalysis, and nanotechnology	Green synthesis	Biomedical, biosensing, and catalytic applications	50
The review discussed the biogenic synthesis of bimetallic nanoparticles with focus on catalytic reduction of 4-nitrophenol	Biological methods	Catalytic reduction of 4-nitrophenol	24

care items.[13] Recent progress in sampling and instrumental techniques has significantly enhanced the sensitivity of analytical instruments, enabling the detection of PPCPs even at minute concentrations.[14] However, conventional wastewater treatment plants (WWTPs) were not originally intended to eliminate PPCPs. Consequently, the majority of existing wastewater treatment technologies fail to achieve complete removal of PPCPs.[15] Nanotechnology offers promising solutions for the environmental remediation of pharmaceuticals and personal care products (PPCPs) in the form of nanostructured materials with enhanced adsorption capacities and catalytic activities, that efficiently capture and degrade PPCPs from contaminated water sources.[16] Nanostructured adsorbents and nano-enable filtration membranes with controlled pore sizes and surface functionalities can selectively remove PPCPs from water streams, while allowing the passage of clean water molecules, thus offering a sustainable approach for water purification.[17] Further, the nanostructured materials degrade PPCPs through advanced oxidation processes, such as photocatalysis and Fenton-like reactions, effectively breaking down pollutants into harmless byproducts.[18] Monometallic nanoparticles, composed of a single metal, have shown significant potential for the remediation of PPCPs due to their unique properties and reactivity.[19] Monometallic nanoparticles possess distinctive physical and chemical properties at the nanoscale such as high surface area with increased surface reactivity facilitating rapid adsorption and degradation of PPCPs, tunable surface chemistry with enhanced PPCPs selectivities, and long-term stabilities, which make them suitable for environmental remediation applications.[20] Monometallic nanoparticles can selectively adsorb PPCPs through electrostatic interactions, hydrogen bonding, and π–π stacking interactions.[21] The surface-functionalized monometallic nanoparticles are incorporated into membrane materials to enhance the removal of PPCPs through size exclusion, electrostatic repulsion, and surface interactions.[22] Monometallic nanoparticles also exhibit catalytic activity in advanced oxidation processes (AOPs) for PPCP degradation. Nanoparticles of metals like palladium (PdNPs) and platinum (PtNPs) can catalyze reactions such as hydrogenation, oxidation, and hydrolysis, leading to the degradation of PPCPs into non-toxic byproducts.[23]

While monometallic nanoparticles have demonstrated efficacy in PPCP remediation, bimetallic nanoparticles comprising of two different metals, offer several advantages that can further enhance remediation processes such as: (a) higher stability and resistance to agglomeration and oxidation compared to monometallic nanoparticles. The presence of multiple metal species stabilizes the nanoparticle structure, thus preventing the surface degradation, and prolonging their lifespan in the remediation applications; (b) exhibiting synergistic effects between the constituent metals, leading to enhanced adsorption and catalytic activity compared to monometallic counterparts. The combination of metals with complementary properties can result in improved reactivity and selectivity for PPCP removal; (c) tailored bimetallic nanoparticles engineered to possess specific surface compositions and electronic structures, allowing enhanced selectivities towards target contaminants, reducing the risk of interference from co-existing pollutants.[24] The bimetallic nanoparticles also offer versatility in terms of composition, morphology, and surface chemistry, allowing the design of tailored nanoparticles optimized for specific PPCP remediation with their adaptation to diverse environmental conditions and pollutant types.[25]

Since the last few decades, bimetallic nanoparticles have attracted the interest of the scientific community for their applications as heterogeneous catalyst and remediation of organic and inorganic contaminants from wastewater (Table 1). However, no review has focused exclusively on the application of bimetallic nanoparticles for the remediation of pharmaceuticals and personal care products (PPCPs) from water. In this comprehensive review, we provide an extensive discussion of the synthetic approaches to get bimetallic nanoparticles with special emphasis on green approaches, their associated morphological traits, techniques used to evaluate those structural features, and the application of bimetallic nanoparticles for PPCPs remediation. Moreover, we also provide a comprehensive summary of the diverse bimetallic nanoparticles used for PPCPs removal, offering a holistic perspective on the subject.

2. Synthesis of bimetallic nanoparticles

Bimetallic nanoparticles are synthesized using top-down and bottom-up approaches. The top-down approach involves breaking down bulk material into nanoscale particles, while the bottom-up approach builds the nanomaterial by mixing metal precursors in specific conditions with reducing or stabilizing agents. Synthesis methods can be classified into physical, chemical, and biological categories. The biological methods of synthesis are also termed as green-approach for the synthesis of bimetallic nanoparticles (Fig. 1).

2.1 Physical methods

Physical methods, part of the top-down approach, break bulk materials into nanoscale particles of two metals, ensuring contamination-free, homogeneously distributed nanoparticles. However, they can be inefficient and produce significant waste. Methods include mechanical grinding, laser ablation, microwave irradiation, and electrical techniques, *etc.*[37]

2.1.1 Mechanical grinding. The mechanical grinding uses high-energy ball or attrition milling to break down metal powders into nanoparticles. This method is scalable and suitable for industrial use, offering controlled composition and size distribution.[51] It has been used to create catalysts like CoFe for CO_2 hydrogenation[52] and NiFe for dechlorination of 4-chlorophenol. Ball-milled Ni–Fe bimetals show superior dechlorination activity compared to those prepared by chemical methods.[53]

2.1.2 Laser ablation. Laser ablation uses laser beams to disintegrate metal targets in liquid, offering precise control over nanoparticle defects, which impact catalytic behavior.[54] This environmentally friendly method avoids the use of reductants and capping agents, producing purer nanoparticles. Laser ablation can create nanoparticles like Ag–Ge[55] and Pt–Au,[56] with the size and properties dependent on factors like laser type and energy.

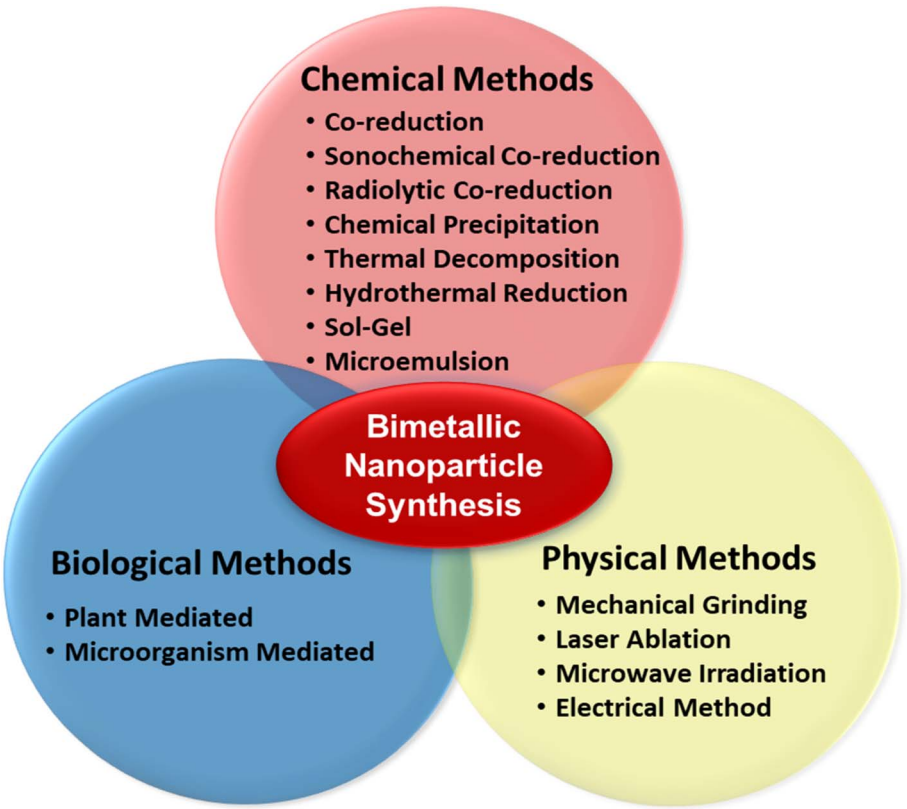

Fig. 1 Schematic of various synthetic approaches for bimetallic nanoparticles.

2.1.3 Microwave irradiation. The microwave irradiation rapidly heats a solution containing metal salts to reduce metal ions and form bimetallic nanoparticles. This method allows for uniform nucleation and size control, improving nanoparticle properties with high reaction speed.[57] Examples include PdNi@VC for enhanced catalysis[58] and CuAg nanoparticles for use in environmental and biomedical applications.[59]

2.1.4 Electrical methods. The electrical methods, including electrochemical and electrospray deposition, use electric current to induce the reduction of metal ions, forming bimetallic nanoparticles. These methods offer precise control over nanoparticle properties and are scalable for applications like catalysis and sensing.[26,38] Studies have shown that electrical deposition can produce Al–Zn nanoparticles with uniform distribution, useful in various industrial applications.[60]

2.2. Chemical method

Chemical methods for synthesizing bimetallic nanoparticles include various approaches designed to control nanoparticle composition, size, and structure. Common methods are:

2.2.1. Simultaneous reduction approach

2.2.1.1 Co-reduction method. Co-reduction is a straightforward method where two metal precursors are mixed, and a reducing or stabilizing agent helps reduce metal ions to atoms and stabilize nanoparticle aggregation. Polymers are often used to regulate the reduction and aggregation. The order of reduction and interactions with stabilizers affect nanoparticle properties.[61] For example, He *et al.* used co-reduction of iron and nickel salts with and without zeolite as support to produce Fe–Ni nanoparticles.[62]

2.2.1.2 Sonochemical co-reduction method. The ultrasound waves create acoustic cavitation in an aqueous mixture, resulting in localized high temperatures and pressures that facilitate nanoparticle growth. Additionally, high-energy radicals are produced to aid the reduction.[63] Mirzajani and Karimi synthesized Ni–Ag nanoparticles stabilized by graphene oxide using sonochemical co-reduction,[64] while ultrasonic irradiation was used for PVP-stabilized Au–Pd nanoparticles.[65]

2.2.1.3 Radiolytic co-reduction method. The radiolytic co-reduction uses ionizing radiation (UV, X-ray, gamma rays) to reduce metal ions and create bimetallic nanoparticles. The process controls nanoparticle growth but is challenging for shaping.[66] Kianfar *et al.* used gamma irradiation to synthesize Pt–M (M = Mo, V, W) nanoparticles,[67] and Treguer *et al.* made Ag–Au nanoparticles with controlled gold cores.[68]

2.2.2 Chemical precipitation method. The chemical precipitation involves dissolving metal ions in a solution and adding reagents to form insoluble nanoparticles, known as co-precipitation when using multiple metal ions.[69] The solution's pH is adjusted, and nanoparticles are collected by centrifugation and dried. Bimetallic nanoparticles produced include Fe–Mn,[69] hBN–Fe_3O_4,[70] Mn–Co,[71] and Fe–Ti.[72]

2.2.3. Thermal decomposition method. Thermal decomposition uses high temperatures to decompose metal precursors. The metal with a lower decomposition temperature reduces first, forming a monometallic nanoparticle, while the second metal deposits on its surface.[28] Bimetallic systems synthesized include M–Ti–O (M = Ni, Co),[73] Pd–Ir,[74] and Co–Mn.[75]

2.2.4 Hydrothermal reduction method. In this method, metal precursors are heated under high pressure in an autoclave to produce high-purity nanoparticles. Parameters like pH, temperature, and pressure can be controlled to adjust nanoparticle properties.[44] Examples include Pd–Au alloys[76] and Ni–Cu nanoparticles.[77]

2.2.5 Sol–gel method. In sol–gel synthesis, metal precursors undergo hydrolysis and polymerization to form a sol, which then transforms into a gel. The process involves hydrolysis, condensation, particle growth, and agglomeration.[78] De León-Quiroz *et al.* synthesized Cu–Ni nanoparticles through this method,[79] and other examples include Mg–Al[80] and Pt–Pd[81] nanoparticles.

2.2.6 Micro-emulsion method. Micro-emulsions involve dispersed droplets of one liquid phase in another, stabilized by surfactants.[82] Water-in-oil (reverse micelles) micro-emulsions are most often used for nanoparticle synthesis.[83] Bimetallic nanoparticles like Au–Pd,[84] Zn–Se,[85] and Pd–Ir[86] were synthesized *via* micro-emulsion.

2.2.7 Successive reduction approach. This method involves multiple reduction steps to control nanoparticle size, shape, and composition. By sequentially reducing metal precursors, it allows for the creation of core–shell bimetallic nanoparticles.[87] In the Au–Ag system, gold can form a core with silver as a shell, while the reverse process may yield hollow nanoparticles due to gold's higher nobility.[88] Examples include Pd–Cu,[61] and Pd–Au,[89] and Pd-core Au–Pt shell nanoparticles.[90]

2.3 Green approach for bimetallic nanoparticles

Traditional synthesis of bimetallic nanoparticles (NPs) *via* physical and chemical methods often requires expensive equipment, produces hazardous by-products, and is time-consuming. The disposal of waste also adds considerable costs. Therefore, there is a need for sustainable, eco-friendly approaches for synthesizing these nanoparticles. Biological methods offer several advantages over chemical and physical methods, such as being eco-efficient, producing non-toxic by-products, utilizing easily accessible bio-resources, and ensuring bio-compatibility.[91] These green approaches mainly involve the use of plant extracts and microorganisms, which contain compounds that facilitate the reduction of metal ions to form nanoparticles.[92]

2.3.1 Microorganism mediated synthesis. Microorganisms can synthesize bimetallic nanoparticles through two mechanisms: extracellular and intracellular. In the extracellular process, metal ions are adsorbed onto the microbe's cell wall, where enzymes reduce them to metallic nanoparticles. The intracellular mechanism, however, involves transporting metal ions into the cell, where they are reduced and transformed into nanoparticles. The nanoparticles are then extracted by breaking the cell wall, making the extracellular process preferable due to its simpler recovery method.[16,93] Despite the abundance of studies on microbial synthesis of metallic nanoparticles,

reports on microorganism-mediated synthesis of bimetallic nanoparticles are limited.

For example, *Shewanella oneidensis* MR1 reduces Pd(II) and Pt(IV) in an anaerobic environment, forming Pd–Pt alloy nanoparticles. This process, which occurs within 24 hours at 30 °C, involves multi-heme c-type cytochromes.[94] The same bacterium has also been used to synthesize Pd–Ag[95] and Pd–Au[96] nanoparticles. Additionally, *Escherichia coli* has been employed to create core–shell Au–Ag,[97] Pd–Au,[98] and Pd–Ru[99] bimetallic nanoparticles. Fungi like *Aspergillus terreus* and *Neurospora crassa* have been used to synthesize Ag–Cu[100] and Au–Ag[101] bimetallic nanoparticles. Yeast and algae have also been explored for synthesizing bimetallic nanoparticles, alongside plant-isolated viral strains like Squash leaf curl China virus (SLCCNV).[102]

2.3.2 Plant mediated synthesis. Plant-mediated synthesis is often considered superior to microbial synthesis due to its simplicity, shorter preparation times, and the stability of plant extracts over time. Plant extracts serve not only as reducing agents but also as stabilizers, preventing nanoparticle oxidation.[103] This method is cost-effective and scalable, making it suitable for large-scale production. However, factors like pH, metal precursor concentration, temperature, and reaction time influence the size and morphology of the nanoparticles.[92] Plant extracts such as *Lemon* (Citrus limon) leaves, *Aloe vera*, and *Redroot lithospermum* have been widely applied for synthesizing various bimetallic nanoparticles, highlighting the versatility of plant-based methods.

For instance, *Cola nitida* (Kolanut) extracts from leaves, seeds, and pods have been used to synthesize Ag–Au bimetallic nanoparticles with various morphologies, such as spheres and rods.[104] *Kigelia africana* fruit extract produced Ag–Cu nanoparticles,[105] while *Moringa oleifera* leaf extract facilitated the synthesis of Ni/Fe_3O_4 nanoparticles.[106] Other plants such as *Azadirachta indica* (Neem) and *Swietenia mahogani* (Mahogany) have been used for synthesizing core–shell Ag–Au nanoparticles.[107,108] *Anacardium occidentale* (Cashew) leaf extract has been employed for Au–Ag alloy synthesis, where temperature and extract concentration were found to influence the nanoparticle stability and size.[109]

Additionally, *Phoenix dactylifera* (palm tree) leaf extract synthesized Cu–Ag nanoparticles,[110] while *Aloe vera* was used to form Ag–Cu nanocomposites when combined with cotton fiber.[111] *Coriander*, *Fenugreek*, and *Soybean* leaf extracts facilitated the synthesis of Au–Ag nanoparticles under controlled heating conditions.[112] Pomegranate fruit juice was also used to create Au–Ag core–shell nanostructures.[113]

Other plant-based synthesis methods include *Terminalia chebula* fruit extract for Ag–Pd bimetallic nanoparticles.[114] *Gum kondagogu*, a biopolymer, was used to synthesize several bimetallic nanoparticles, including Au–Ag and Ag–Pd.[115] Additionally, *Ixora finlaysoniana* (Ixora) plant extract was employed for Fe–Cu nanoparticle synthesis,[116] and *Henna* (Lawsonia inermis) seed extracts were used in ultrasound-assisted synthesis of Au–Ag nanoparticles.[117] Moreover, the leaf extract of *Piper pedicellatum* facilitated the synthesis of Ag–Au nanoparticles,[118] and *Nigella sativa* (black seed) extract was used for Pd–Ag nanoparticle synthesis (Fig. 2).[119]

2.4. Polymer-mediated bimetallic nanoparticles synthesis

Bio-extracts are complex mixtures of organic compounds, which can introduce variability and difficulty in standardizing the process. Bio-extracts may contain impurities or unwanted organic materials that could affect the properties or stability of the bimetallic nanoparticles. Therefore, more sustainable biocompatible polymeric materials may be employed which do not cause adverse reactions in biological systems. They are non-toxic, non-immunogenic, biodegradable, and have the mechanical strength needed for biomedical use. Examples include polyethylene glycol (PEG), polylactic acid (PLA),

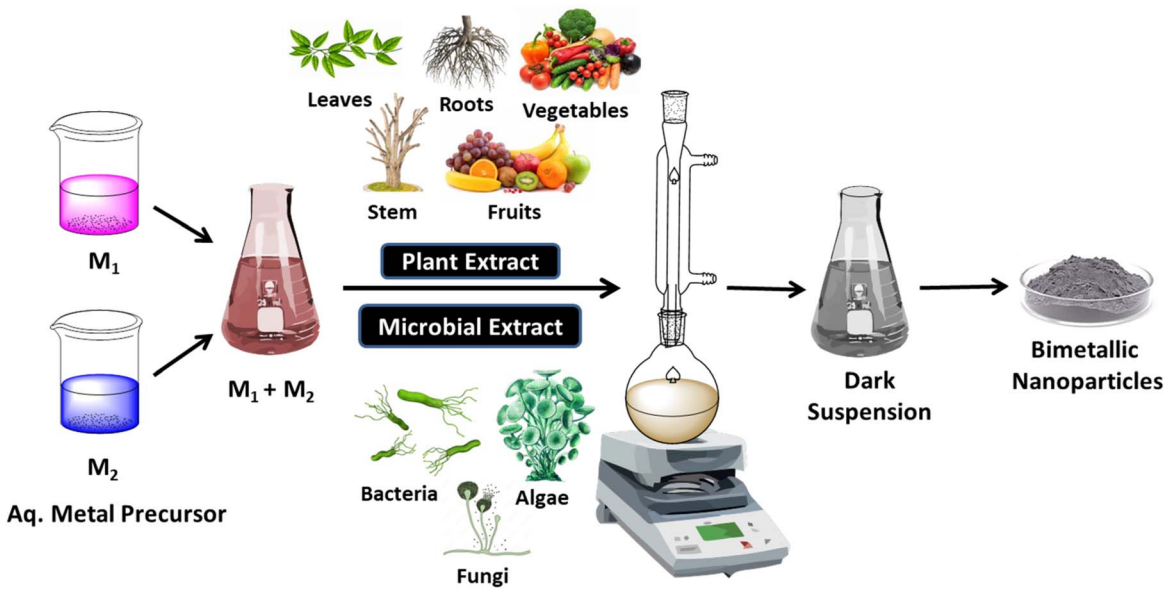

Fig. 2 Green synthesis of bimetallic nanoparticles.

poly(lactic-*co*-glycolic acid) (PLGA), polyethylene oxide (PEO), and chitosan.[120] In nanoparticle synthesis, these polymers act as templates or stabilizers. Their functional groups coordinate with metal ions to promote reduction and nanoparticle growth. The polymers provide a controlled environment for nucleation and growth, resulting in bimetallic nanoparticles with tailored properties.[121] The process involves mixing metal precursors and polymer in a solvent, followed by adding reducing agents to form and stabilize nanoparticles.[122]

2.5. Solid-supported bimetallic nanoparticles synthesis

This category refers to bimetallic nanoparticles anchored onto a solid support, which not only prevent the aggregation but also contribute to the stability and durability of the nanoparticles. Solid support may include materials like silica, alumina, or carbon.[123] These solid-supported bimetallic nanoparticles find extensive application in the catalytic processes, including hydrogenation, oxidation, and reduction reactions.[33]

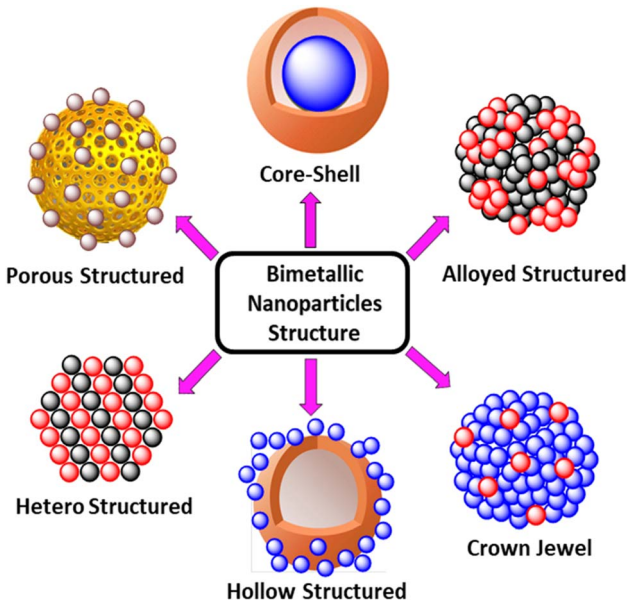

Fig. 3 Structure of bimetallic nanoparticles.

3. Structure of bimetallic nanoparticles

The bimetallic nanoparticles exhibit diverse shapes and sizes depending on the synthetic approaches employed during their production (Fig. 3). Further, the presence of capping or stabilizing agents during formation not only reduce the metal salts to their bimetallic form, but also prevent the nanoparticles from agglomerating by creating a steric or electrostatic repulsion between the particles, thus play a crucial role in determining the structure, size, and stability of bimetallic nanoparticles (NPs). The various stabilizing agents used for the synthesis of bimetallic nanoparticles include polyvinylpyrrolidone, citrates, sodium dodecyl sulfate, cetyltrimethylammonium bromide, oleic acid, ionic liquids, bovine serum albumin, chitosan, *etc.*[124] By controlling the growth rate of different crystal faces, capping agents can influence the overall shape and size of the bimetallic NPs. The structure of bimetallic nanoparticles (such as core–shell, alloy, or segregated structures) can be influenced by the type and distribution of capping agents on the surface. In bimetallic nanoparticles, capping agents can help in the proper interaction between the two metals, preventing unwanted phase separation or ensuring uniform alloying.[125] Several typical morphologies of bimetallic nanoparticles have been observed, including:

(a) Crown jewel structure: in this architectural setup, a single metal atom (referred to as the "jewel" atom) is carefully arranged on the surface of another metal. The "jewel" metal is typically a precious and catalytically active one, such as gold (Au), silver (Ag), or platinum (Pt). Zhang *et al.* prepared Pt–Au bimetallic nanoparticle synthesis by galvanic replacement reaction method having Crown Jewel structure morphology[126] (Fig. 4).

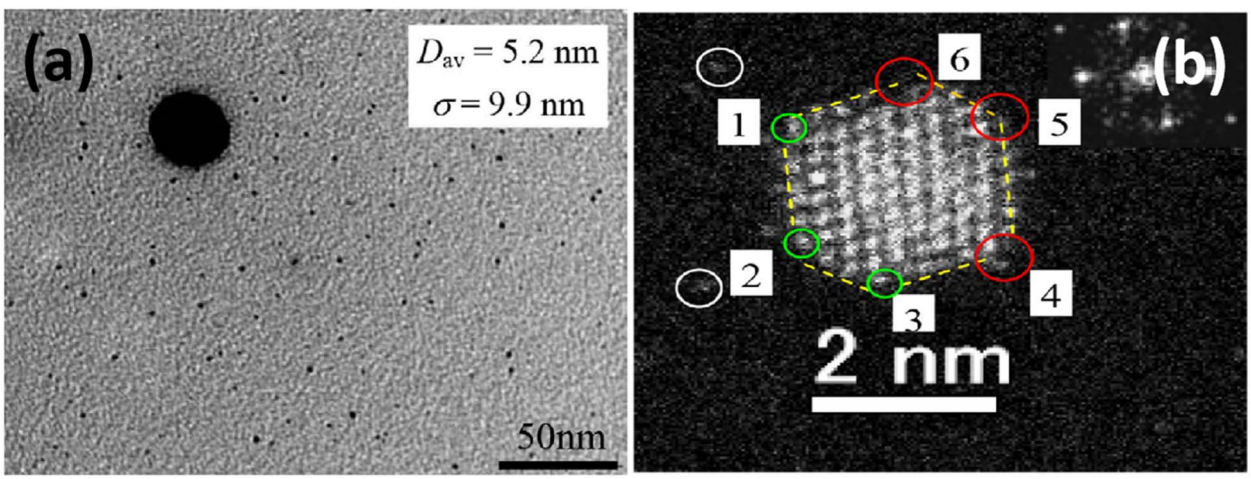

Fig. 4 (a) TEM micrograph of crown jewel Pt/Au NCs; (b) high-angle annular dark-field scanning TEM (HAADF-STEM) image of a single crown jewel Pt/Au NCs[126] (reproduced under Creative Commons Attribution (CC BY) license http://creativecommons.org/licenses/by/4.0/).

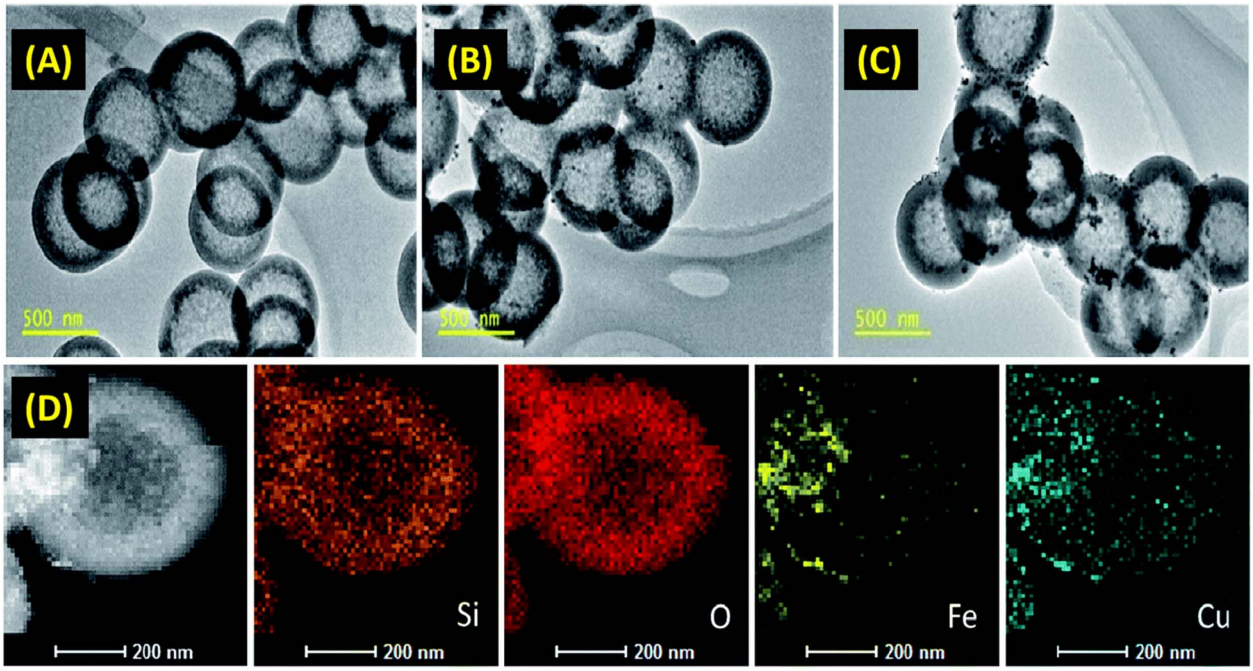

Fig. 5 TEM of (A) blank hollow mesoporous silica sphere; (B) Fe loaded hollow mesoporous silica sphere; (C) Fe–Cu bimetallic hollow mesoporous silica sphere; (D) STEM and elemental mapping images of Fe–Cu bimetallic hollow mesoporous silica sphere[127] (reproduced with permission, RSC Publishing, 2016).

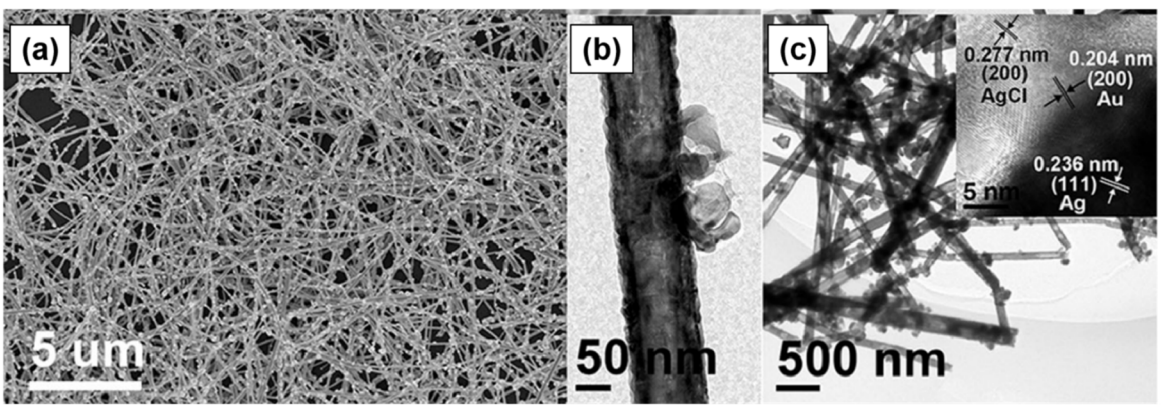

Fig. 6 (a) SEM image of Ag–Au/AgCl hollow heterostructures; (b) the enlarged TEM image of a single Ag–Au/AgCl nanowire. (c) TEM image of Ag–Au/AgCl hollow heterostructures (inset: HRTEM image of Ag–Au/AgCl hollow heterostructure)[128] (reproduced under Creative Commons Attribution (CC BY) license http://creativecommons.org/licenses/by/4.0/).

(b) Hollow structure: to synthesize hollow bimetallic nanoparticles a template which is a sacrificial material is fabricated on which the metals can deposit by methods such as chemical reduction, electrochemical deposition, or physical vapor deposition. The removal of the template leaves behind a hollow structure with bimetallic nanoparticles. The choice of metals and deposition conditions determines the composition and properties of the resulting hollow nanoparticles. Wang *et al.* prepared Fe–Cu bimetallic nanoparticle synthesis by direct impregnation and chemical reduction method having hollow structure morphology[127] (Fig. 5).

(c) Hetero structure: heterostructure bimetallic nanoparticles refer to the nanostructures consisting of two different metals with distinct compositions, and precise control over the arrangement often achieved through sophisticated fabrication techniques such as seed-mediated growth, galvanic replacement, or chemical deposition, *etc.* These nanoparticles exhibit unique properties derived from the combination of the two metals, offering enhanced performance for various applications. Liu *et al.* prepared Ag–Au bimetallic nanoparticle having hetero structure morphology[128] (Fig. 6).

(d) Core–shell structure: core–shell bimetallic structures consist of one metal forming the core, encapsulated or

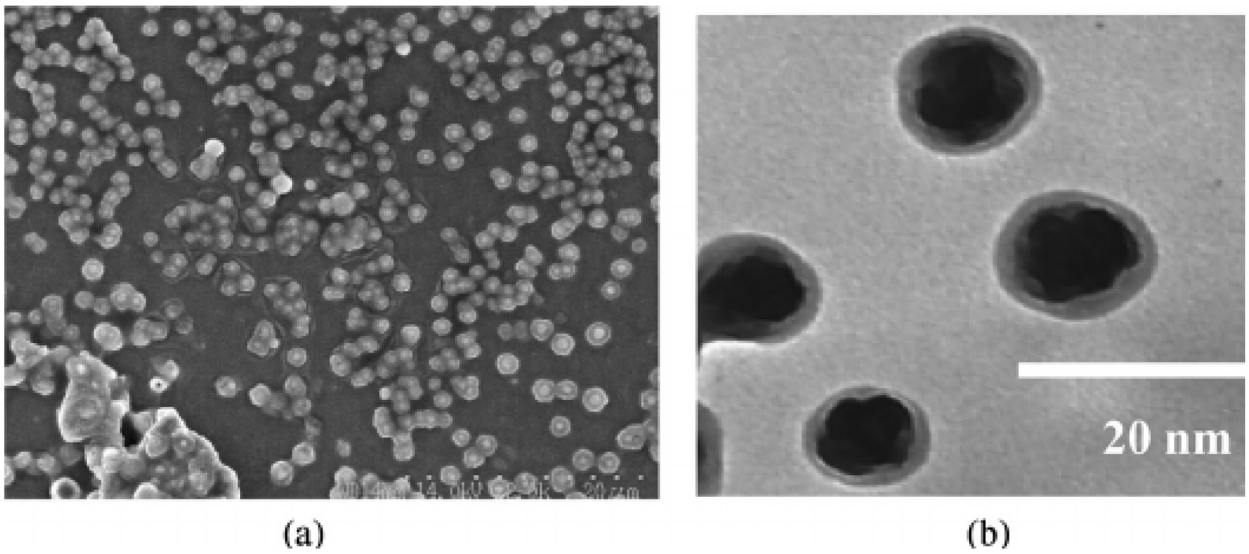

Fig. 7 (a) SEM; and (b) TEM images of bimetallic Ru–Ni nanoparticles with core-and-shell structure (Ru in core and Ni in the shell)[129] (reproduced with permission, Taylor & Francis, 2007).

surrounded by another metal forming the shell. The synthesis involves controlled deposition of the shell material onto the core, achieved through methods like chemical reduction, electrochemical deposition, or atomic layer deposition. Pingali *et al.* prepared Ru–Ni bimetallic nanoparticle synthesis by wet-chemistry method having core–shell morphology[129] (Fig. 7).

(e) Alloyed structure: an alloyed bimetallic structure refers to a homogeneous mixture of two different metals at an atomic

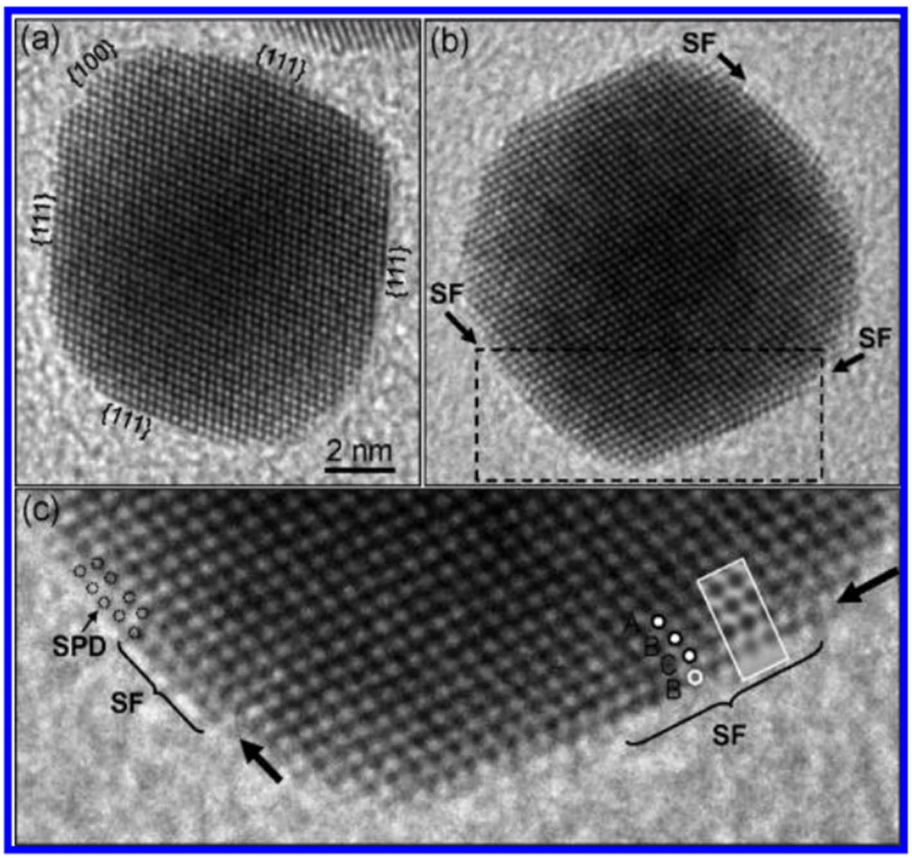

Fig. 8 HRTEM images of (a) Au seed; (b) alloyed bimetallic nanoparticle with single atomic layer of Pd; and (c) magnified HRTEM image from the rectangle-enclosed area in (b)[130] (reproduced with permission, ACS Publisher, 2010).

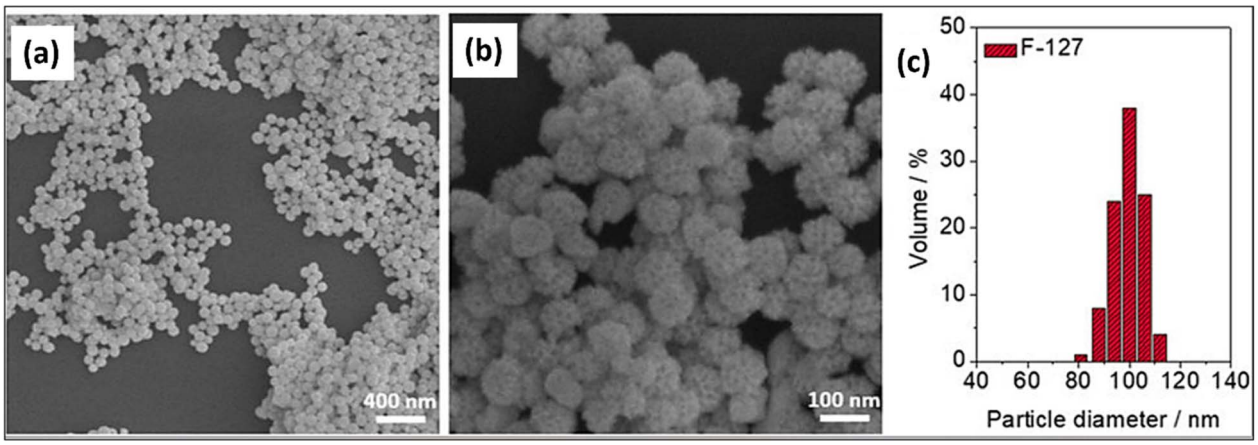

Fig. 9 (a) SEM images of porous Pd@Pt NPs; (b) magnified image; (c) particle size distributions of Pd@Pt NPs[131] (reproduced with permission, Elsevier, 2019).

level, resulting in a single solid phase with properties distinct from those of its individual components. For synthesizing alloyed bimetallic structures, two metals are mixed in controlled ratios and conditions, often through methods such as co-reduction, co-precipitation, or alloying during thermal treatment. Ding *et al.* prepared Au–Pd (gold–palladium) bimetallic nanoparticle synthesis by seed-mediated growth method having alloyed morphology[130] (Fig. 8).

(f) Porous structure: porous bimetallic structures are characterized by having void or pores within their composition, resulting in increased surface area and enhanced reactivity. The synthesis of porous bimetallic structures involves techniques like templating, dealloying, or etching, where sacrificial templates or selective removal of one of the metals from an alloy creates the porous structure. Shim *et al.* prepared Pd@Pt (palladium–platinum) bimetallic nanoparticle synthesis by soft-template method having porous morphology[131] (Fig. 9).

4. Characterization techniques of bimetallic nanoparticles

The arrangement, shape, size, composition, and surface properties of bimetallic nanoparticles significantly influence their behavior and applications. Understanding the atomic structure and bonding patterns aids in predicting their properties and performance in various fields.[92] A range of techniques are used to characterize these nanoparticles and evaluate their unique properties. Some key methods include:

(a) Morphological traits: the shape, size, and surface structure of bimetallic nanoparticles play a pivotal role in determining their reactivity and functionality in various applications. Techniques such as Dynamic Light Scattering (DLS) are widely used to measure particle size,[132] while Transmission Electron Microscopy (TEM) and Scanning Electron Microscopy (SEM) offer detailed insights into the nanoparticle structure and morphology.[133] Scanning Tunneling Microscopy (STM) and Atomic Force Microscopy (AFM) also provide high-resolution imaging and topographical analysis,[134,135] enabling the assessment of surface features and particle distribution.

(b) Topology: the distribution and arrangement of the two metals within the nanoparticle are crucial in defining its overall properties. X-ray Diffraction (XRD) is commonly used to study the crystallinity and phase composition, helping determine the crystalline structure and phase separation of the metals.[136] TEM can also provide topological insights by revealing the internal arrangement. Zeta potential measurements help determine the charge distribution and stability of the nanoparticles,[137] while Brunauer–Emmett–Teller (BET) analysis is useful for evaluating the surface area and porosity.[138]

(c) Chemical properties: chemical properties such as reactivity, catalytic behavior, and surface chemistry are central to the performance of bimetallic nanoparticles. Techniques like UV-Visible Spectroscopy (UV-vis) provide valuable information on optical properties and electronic structure. Energy-Dispersive X-ray Spectroscopy (EDXS) offers elemental composition data, while Fourier Transform Infrared Spectroscopy (FTIR) helps identify functional groups and surface interactions.[118,139]

(d) Electrical properties: the electrical behavior of bimetallic nanoparticles is essential in applications like electronics and sensors. AC/DC conductivity measurements are used to evaluate the electrical conductivity and resistivity,[140] while electrokinetic studies, such as zeta potential and cyclic voltammetry, help assess the charge dynamics and surface electrochemical properties.[141]

(e) Optical properties: optical characteristics such as absorption, scattering, and plasmonic resonance are crucial for applications like sensing, imaging, and photothermal therapy.[142] Microscopy, FTIR, UV-Vis, Raman spectroscopy, and surface plasmon resonance (SPR) are commonly used techniques to study the optical properties of bimetallic nanoparticles.[143,144]

(f) Thermal properties: the ability of bimetallic nanoparticles to conduct heat and their stability at elevated temperatures are critical for heat transfer and catalysis. Thermal analysis

methods like Differential Scanning Calorimetry (DSC),[145] Thermogravimetric Analysis (TGA), and Differential Thermal Analysis (DTA) are used to measure properties such as thermal conductivity, heat capacity, and melting points.[146]

(g) Magnetic properties: magnetic behavior such as magnetization, susceptibility, and coercivity are important for applications like magnetic storage, imaging, and cancer treatment. Vibrating Sample Magnetometry (VSM),[147] Superconducting Quantum Interference Device (SQUID),[148] and Magnetic Force Microscopy (MFM)[149] are employed to analyze the magnetic characteristics of bimetallic nanoparticles.

(h) Mechanical properties: the mechanical strength, elasticity, hardness, and ductility of bimetallic nanoparticles are essential for their integration into nanocomposites and other materials. AFM and thermomechanical analysis are used to assess the mechanical properties of nanoparticles, which are important for applications that require durability and structural integrity.[150]

5. Mechanism of bimetallic nanoparticle mediated remediation of pharmaceutical

The mechanism of pharmaceutical remediation by bimetallic nanoparticles typically involves five steps:

(a) Adsorption: pharmaceuticals in water or soil typically exist in the form of dissolved molecules. Bimetallic nanoparticles having a high surface area-to-volume ratio, provides ample active sites for the adsorption of pharmaceutical molecules on its surface through various interactions, such as hydrogen bonding, van der Waals forces, and electrostatic interactions.[187]

(b) Chemical transformation: once the pharmaceutical molecules are adsorbed onto the surface of the bimetallic nanoparticles, these can undergo chemical transformations through various advanced oxidation processes involving reactive oxygen species such as $SO_4^{\bullet -}$, $^{\bullet}OH$, $O_2^{\bullet -}$, $^1O_2$, *etc.* The presence of two different metals in the bimetallic nanoparticle structure can lead to synergistic effects, enhancing the catalytic activity and selectivity of these reactions. This chemical transformation may involve processes such as oxidation, reduction, hydrolysis, or other reactions facilitated by the unique electronic and chemical properties of the bimetallic nanoparticles.[169]

(c) Degradation: the chemical transformations facilitated by the bimetallic nanoparticles often result in the degradation of the pharmaceutical molecules into simpler and less toxic compounds, such as carbon dioxide, water, and other harmless byproducts.[201]

(d) Release of byproducts: after degradation, the byproducts or transformed molecules may remain adsorbed onto the surface of the bimetallic nanoparticles or are released into the surrounding environment. The release kinetics of these byproducts may depend on the various factors, such as the affinity of the byproducts for the nanoparticle surface, environmental conditions (*e.g.*, pH, temperature), and the nature of the surrounding matrix (*e.g.*, water, soil).[18]

(e) Regeneration: in some cases, the bimetallic nanoparticles may lose their activity over time due to catalytic poisoning. The regeneration strategies, such as washing with appropriate solvents or rejuvenation through treatment with oxidizing or reducing agents, can help restore the activity of the nanoparticles and prolong their lifespan for continued pharmaceutical remediation (Fig. 10).[165]

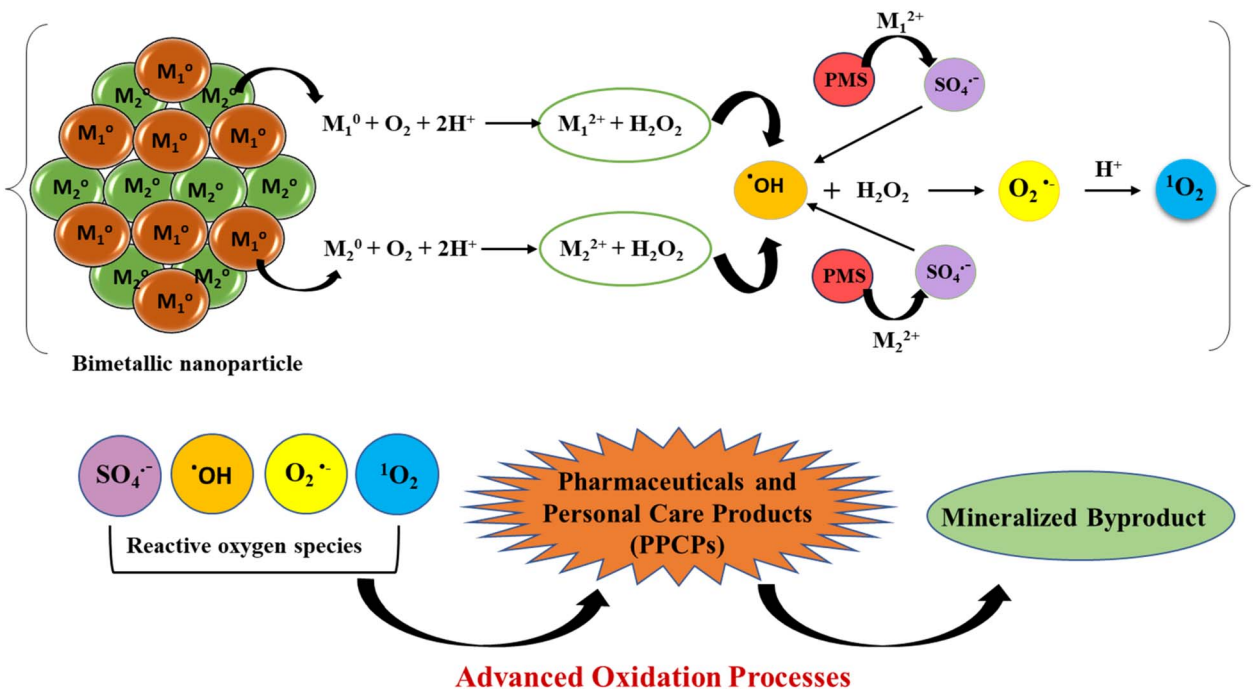

Fig. 10 Schematic representation of bimetallic nanoparticle mediated remediation of pharmaceutical by advanced oxidation processes.

6. Applications of bimetallic nanoparticles for PPCPs remediation

Bimetallic nanoparticles have diverse applications across various fields due to their unique properties and synergistic effects arising from the combination of two different metals. Some of the significant applications of bimetallic nanoparticles include organic catalysis,[123] biomedical applications,[151] electronics, sensors and optoelectronics,[152] surface-enhanced Raman spectroscopy (SERS),[153] and energy applications.[33] Through their unique catalytic, adsorptive, and reactive properties bimetallic nanoparticles are employed for the

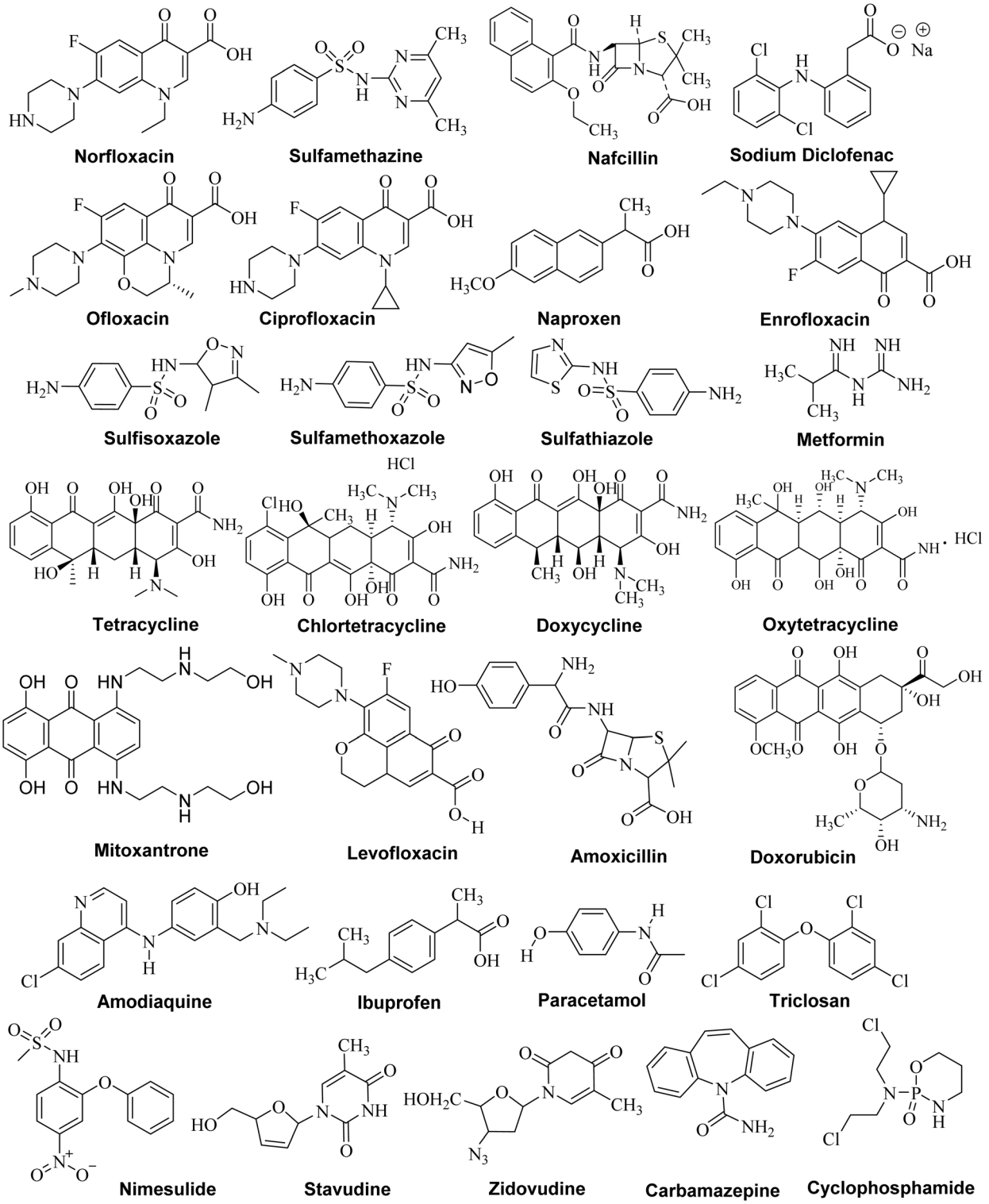

Fig. 11 Structure of various pharmaceuticals used as PPCPs.

Table 2 Bimetallic nanoparticles mediated remediation of pharmaceuticals

			Optimum experimental conditions				
Bimetallic (BM) nanoparticles	Pollutant	Contaminant (mg L^{-1})	BM dose (g L^{-1})	pH	Time (min)	Removal (%)	Ref.
Co–Fe	Amoxicillin	1096.2	0.1	7	30	100	200
Fe–Ni	Amoxicillin	29.45	0.58	2	76.32	85	202
Co–Ag	Amoxicillin	100	0.2	7	30	99.1	201
Fe–Ni@Cs	Amoxicillin	30	1.25	4	80	69	202
Co_xZn_y-JUC-160	Amodiaquine	250	0.005	4	240	99	198
Fe–Cu	Carbamazepine	5	0.4	5	20	95	209
Fe–Cu	Ciprofloxacin	20	8.0	6	40	97.3	168
Fe–Cu@PVP	Ciprofloxacin	100	0.5	6	120	95.6	169
Fe–Cu@rGO	Cyclophosphamide	20	0.5	3	60	80	177
JLUE-MOG-Fe/Y	Chlortetracycline	20	1.0	6	720	90	213
Fe–Cu@CS	Diclofenac	25	0.5	5	20	92	195
Fe–Cu@SBC	Diclofenac sodium	20	0.1	6.9	60	99.7	214
Fe^0–M^0@Fe^0	Diclofenac	9.5	40	7.5	10	80	197
g-C_3N_4@Fe–Pd	Doxorubicin	90	0.2	7	30	75.3	204
Fe–Ni	Doxorubicin	100	0.5	7	20	84	205
Fe–Zn	Doxycycline	20	0.05	3	20	95.5	185
Fe–Cu@C	Enrofloxacin	20	0.02	3.6	60	94	172
Fe–Cu@N–C	Enrofloxacin	20	0.02	3.6	60	92	172
Fe–Cu	Levofloxacin	10	8.0	7	45	100	168
(Fe–Cu)	Metformin	10	0.2	5	30	73	207
Fe–Pd@g-C_3N_4	Mitoxantrone	12	0.02	7	180	92.3	157
Fe–Cu	Nafcillin	0.05	0.036	7	10	88	208
Fe–Cu@CS	Naproxen	25	0.5	5	20	84	195
Ni–Fe@SiO_2	Nimesulide	40	6.0	11.7	15	100	162
Fe–Ni	Nimesulide	45	0.2	11.7	5	60	163
Fe–Cu	Norfloxacin	20	—	3	90	98.64	165
Co–Zn	Norfloxacin	50	0.01	6	150	85.1	166
Fe–Cu	Ofloxacin	30	1	9	240	92	173
Fe–Ni@ZIF-8	Oxytetracycline	10	0.25	7	160	74.6	189
Pd–Fe@rGO	Oxytetracycline	100	0.1	5	60	96.5	190
Fe^0–Cu	Paracetamol	10	0.5	5	45	86	160
Ag–Au	Stavudine	—	0.02	—	15	95.76	175
Ag–Cu	Stavudine	—	0.02	—	15	91.78	175
Au–Cu	Stavudine	—	0.02	—	15	86.61	175
Fe–Cu	Sulfamethazine	5	0.08	6	60	87	192
ZnO–SnO_2	Sulfamethoxazole	10	0.06	7	120	88	193
Fe^0–C@Cu	Sulfathiazole	20	0.5	3	180	97.1	179
ZnO–SnO_2	Sulfisoxazole	10	0.06	7	120	88	193
Fe–Zn@HEC-GO (Fe : Zn, 1 : 1)	Tetracycline	20	0.05	4	100	85	180
Fe–Zn@HEC-GO (Fe : Zn, 2 : 1)	Tetracycline	20	0.05	4	20	95	185
Co_3O_4–Fe_3O_4	Tetracycline	50	3.0	9	420	99.43	182
Fe–Cu@B	Tetracycline	10	0.75	7	90	95	183
Fe–Ni	Triclosan	10	1.5	6	180	75.8	211
Fe–Co	Triclosan	5	1.12	6.92	15	99.8	212
Ag–Au	Zidovudine	—	0.02	—	15	91.45	175
Ag–Cu	Zidovudine	—	0.02	—	15	87.98	175
Au–Cu	Zidovudine	—	0.02	—	15	85.41	175

remediation of environmental pollutants such as organic contaminants and heavy metals.[42] Their high surface area-to-volume ratio and tunable surface chemistry make them effective in accelerating degradation reactions, such as oxidation or reduction processes.[154] Bimetallic nanoparticles can facilitate the reduction of toxic metals like chromium, arsenic, and mercury into less harmful forms.[155] Among the various contaminants that pose serious threat to environment, pharmaceuticals and personal care products (PPCPs) are among the most concerning due to their capacity to bioaccumulate and biomagnify within aquatic organisms. This part of the review provides comprehensive evaluation of various bimetallic nanoparticles and their composites used for the PPCPs remediation from water and soil (Fig. 11) (Table 2).

Mitoxantrone, an anthracenedione class of medications treats multiple sclerosis by impeding specific immune cells from accessing the brain and spinal cord, thus averting damage. In cancer treatment, Mitoxantrone halts the proliferation and dissemination of cancerous cells.[156] However, Mitoxantrone (MTX) poses significant environmental risks due to its potential

genotoxic and mutagenic effects on both aquatic organisms and humans.[84] Xu *et al.* employed the hybrid nanomaterial (Fe–Pd@g-C_3N_4) for the removal of mitoxantrone (MTX), an antibiotic and antitumor drug, achieving a removal efficiency of 92.0% with a removal capacity of 450 mg g^{-1}. The MTX aqueous solution on exposure to the hybrid material, gradually changed the color from dark blue to lighter shades. The liquid chromatography-UV detection (LC-UV) of residual solutions revealed a new peak at 3.0 min (compared to MTX's peak at 13.2 min) after the removal by Fe–Pd@g-C_3N_4, indicating the presence of intermediate products and also confirming the MTX degradation. The detailed mass spectrometric analysis showed a decrease in nuclear mass ratio from *m*/*z* 445.2 (M + 1H) to *m*/*z* 126.0, 169.1, 239.2, 267.3, 285.2, 371.4, and 415.2 representing the degradation of MTX and formation of degradation of products. The component with the highest proportion among all the degradation products with *m*/*z* (126.0 (M + 1H)) was found to be 40–100 times less toxic than the MTX, comprising 5.63% of all the degradation products. The analysis of degradation products assisted in the proposed mechanism outline for the removal and degradation of MTX. Real water experiments confirmed that Fe–Pd@g-C_3N_4 can achieve a maximum removal capacity of MTX up to 492.4 mg g^{-1} (at 0.02 g L^{-1}, 10 ppm).[157]

Ibuprofen, a non-steroidal anti-inflammatory drug (NSAID), alleviates pain, fever, and inflammation, and treats various conditions, including closing a patent ductus arteriosus in premature infants, while also harming aquatic organisms due to cytotoxic and genotoxic damage, elevated oxidative cell stress, and unfavorable effects on growth, reproduction, and behavior.[158] In their recent investigation, Rout *et al.* present a surfactant-assisted deposition coreduction method for synthesizing non-noble bimetallic nanoparticles supported on graphitic carbon nitride (g-C_3N_4). This nanocomposite was utilized for the H_2 gas evolution through water splitting and efficient photocatalytic wastewater treatment *via* ibuprofen (IBU) degradation studies. The structural and morphological analysis confirmed the uniform distribution of Cu–Co bimetallic nanoparticles over g-C_3N_4, without any aggregation. The Cu–Co alloy bimetallic nanoparticle combination was confirmed by the even distribution of elemental Cu and Co observed in energy-dispersive X-ray (EDX) studies. The optical and electrochemical assessments revealed enhanced photoresponse properties, reduced charge recombination, and prolonged lifespan of the composite. The recyclable nanocomposite efficiently degrades the hazardous pharmaceutical contaminant ibuprofen (IBU) (k_{app} = 0.02 min^{-1}). Further, the cytotoxicity of IBU after photocatalytic degradation was evaluated against Gram-negative *P. aeruginosa* and Gram-positive *B. subtilis* bacteria using the 5 wt% Cu–Co (3 : 1)/g-C_3N_4 nanocomposite.[159]

Paracetamol, a non-opioid analgesic and antipyretic, treats fever and mild to moderate pain. Its environmental persistence raises concerns regarding bioaccumulation and biomagnification. Abd El-Aziz *et al.* performed biogenic synthesis of bimetallic zero-valent iron/copper (Fe^0–Cu) nanoparticles using a green approach with *Ficus benjamina* leaf extract and studied for the removal of paracetamol from aqueous medium. The synthesis and surface morphology of bimetallic nanoparticles was evaluated using energy-dispersive X-ray (EDX) spectroscopy, scanning electron microscopy (SEM), and Fourier transform infrared spectroscopy (FTIR). At a concentration of 10 mg L^{-1}, the paracetamol removal efficiency reached 86% under the conditions of 0.5 g L^{-1} dose, 45 min reaction time, and pH of 5. The Fe^0–Cu nanoparticles exhibited significant durability and stability for the paracetamol removal even after five cycles of reusability. Langmuir adsorption isotherm model (R^2 = 0.9989) provided the best fit of the equilibrium adsorption data with a maximum adsorption capacity (q_{max}) of 16.49 mg g^{-1}. The adsorption kinetics followed a pseudo-second-order model. The linear regression analysis of functional parameters revealed their significant influence and explained over 98% of the variables affecting the removal process.[160]

Nimesulide, a moderately COX-2 selective NSAID, provides analgesic and antipyretic effects. Approved uses include treating acute pain, osteoarthritis symptoms, and primary dysmenorrhoea in adolescents and adults. It is commonly detected in sewage and terrestrial water and causes chronic poisoning of aquatic organisms.[161] Gonçalves *et al.* synthesized silica-supported bimetallic nanoparticle assemblies composed of Ni and Fe (Ni–Fe@SiO_2), ranging in diameter from 20 to 200 nm and utilized for the reductive degradation of nimesulide in aqueous solution. The SEM analysis confirmed the uniform anchoring of the nanoparticles on silica, while EDS analysis indicated the presence of Fe, Ni, and silica, and XRD analysis revealed the presence of Fe^0 and Fe_2O_3/Fe_3O_4 structures. The complete removal of nimesulide (50 mg L^{-1}) was achieved using 8 wt% Ni silica-supported bimetallic nanoparticles (6 g L^{-1}) after 15 min of reaction. The evaluation of external and internal mass transfer, and a theoretical analysis of the reductive reaction demonstrated that the degradation of nimesulide involves the reduction of the nitro group and removal of the sulfonyl group, resulting in the formation of an amine and thioester aromatic derivative product.[162] Araújo *et al.* employed the carboxymethyl cellulose (CMC) stabilized Fe–Ni bimetallic nanoparticles (CMC–bNP–Fe–Ni) to facilitate the reductive degradation of the drug nimesulide (NMS) in both aqueous solution and secondary effluent. It was observed that the nanoparticles containing 17 wt% of Ni exhibited optimal performance for NMS degradation, achieving the complete removal of NMS with the formation of aromatic by-products across NMS concentrations ranging from 10 to 60 mg L^{-1} using CMC–bNP–Fe–Ni (0.2 g L^{-1}). Further, the observed higher NMS removal rates with increasing concentrations of both CMC–bNP–Fe–Ni and NMS corresponded to the heterogeneous reaction under agitated conditions. The investigation of the degradation of NMS in the presence and absence of dissolved oxygen demonstrated the impact of oxygen's on the process for NMS concentrations <45 mg L^{-1}. The comparative analysis of NMX removal with CMC–bNP–Fe–Ni, bNP–Fe–Ni, and the carboxymethyl cellulose stabilized zero-valent iron nanoparticles (CMC–Fe) revealed the superior NMS degradation levels achieved solely with the CMC–bNP–Fe–Ni system, mainly through the reduction of nitro and sulfonyl groups, leading to the

formation of aromatic by-products. Further, the reductive treatment of secondary effluent with CMC–bNP–Fe–Ni caused rapid reduction in NMS concentration, achieving a percentage reduction of 95% within 5 min of contact time.[163]

Norfloxacin, marketed as Noroxin, is a fluoroquinolone antibiotic treating urinary, gynecological infections, prostatitis, gonorrhea, and cystitis. It considered an emerging pollutant owing to its low degradation and has many side effects on human vitals.[164] Heterogeneous electro-Fenton (H-EF) emerges as a promising solution for eliminating persistent organic pollutants, highlighting the critical need for efficient cathodes. In their recent investigation, Du *et al.* introduced a stable cathode, FC12-NC@CF, derived from Fe–Cu–N doped carbon felt, to facilitate the norfloxacin removal *via* heterogeneous electro-Fenton reaction. The synthesis of FC12-NC involved the carbonization in a nitrogen environment, resulting in its characteristic rod-like morphology originating from the Fe–Cu bimetal MOF. This cathode exhibited a synergistic effect between Fe and Cu, thus promoting electron transfers and significantly enhancing the oxygen reduction reaction (ORR) for a two-electron process ($n = 2.13$). The efficient norfloxacin (NOR) removal was achieved within 90 min across a wide pH range (pH 3–9), while the modified cathode displayed an exceptional stability and catalytic performance over six recycles of reusability. The H-EF process was proposed to operate through the formation of hydroxyl radicals (˙OH) as the primary active species. The toxicity assessment using the Toxicity Estimation Software Tool (T.E.S.T.) suggested a partial decrease in NOR toxicity following the H-EF reaction.[165] Wang *et al.* utilized magnetic nitrogen-doped porous carbon prepared through a self-catalytic pyrolysis of bimetallic metal–organic frameworks (MOFs). The resulting (Co–Zn, MNPC) exhibited favorable characteristics for the antibiotic's adsorption, including a high specific surface area (871 $m^2 g^{-1}$), high pore volume (0.75 $cm^3 g^{-1}$), porous structure, well-developed graphitization, and the abundant N-doping. The presence of Co species imparted magnetic properties to the MNPC, facilitating easy separation of the adsorbent due to their high dispersion. Using these properties, the MNPC was employed as an adsorbent for the norfloxacin (NOR) removal from aqueous medium. The experimental findings revealed a maximum NOR adsorption capacity of 55.12 mg g^{-1} at 298.15 K and pH 6.0, with an initial NOR concentration of 50 mg L^{-1}. The kinetic analysis exhibits a strong agreement with the pseudo-second-order model, while isotherm data analysis favored the Freundlich model. The adsorption experiments conducted under various conditions decided the pore-filling, electrostatic interaction, and the hydrogen bonding as the primary adsorption mechanisms.[166]

Ciprofloxacin and Levofloxacin, both fluoroquinolone antibiotics, are prescribed for bacterial infections such as bone and joint, intra-abdominal, respiratory, and urinary tract infections. However, these emerging micro-pollutant antibiotics, poses a serious environmental threat due their resistance to high-temperature decomposition, and aiding antibiotic resistance spread.[167] Ahmad *et al.* performed the preparation of bimetallic nanoparticles Fe–Cu on the Alginate-limestone support, with an aim to increase the surface area in Fe–Cu@Alg–LS nanocomposite. The surface morphology, particle size, crystallinity

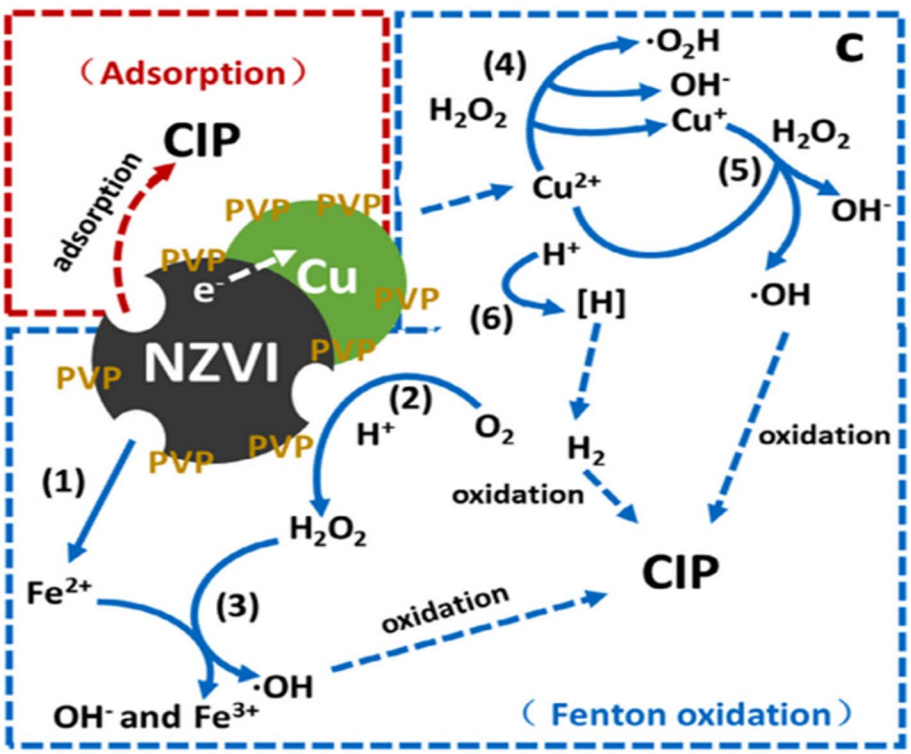

Fig. 12 Schematic model for ciprofloxacin removal by Fe–Cu@PVP bimetallic particles under oxic condition[169] (reproduced with permission, Elsevier, 2019).

percentage, and elemental content of the nanocomposite were evaluated using SEM, EDX, and TEM analysis. Fe–Cu@Alg–LS was employed as an adsorbent for the removal of pharmaceuticals like ciprofloxacin (CIP) and levofloxacin (LEV) from contaminated media. The adsorption parameters determined using kinetic and isotherm models, exhibits maximum removal efficiencies of 97.3% for CIP (20 ppm) and 100% for LEV (10 ppm). The optimal conditions included pH 6 and 7 for CIP and LEV, contact times of 45 and 40 min, respectively at 303 K. The pseudo-second-order model, indicating chemisorption, and the Langmuir model were found to be the most suitable kinetic and isotherm models, respectively.[168] Chen *et al.* devised a novel catalytic system by integrating the polyvinylpyrrolidone (PVP) and nanoscale zerovalent iron (nZVI) with copper (Cu) bimetallic particles, denoted as Fe–Cu@PVP, aimed at reducing ciprofloxacin (CIP) under the influence of a weak magnetic field (WMF). The catalytic efficacy of Fe–Cu@PVP was evaluated both in the presence and absence of WMF. The experimental outcomes revealed that the Fe–Cu@PVP composite when subjected to WMFa exhibits a significant enhancement in the catalytic performance, achieving a maximum CIP removal rate of 95.6% within 120 min. The kinetic analysis illustrated that the degradation of CIP followed the pseudo-first-order kinetics. Mass spectrometry (MS) was employed to identify the degradation products of CIP upon interaction with the Fe–Cu@PVP nanocomposites. The quantitative assessment of Fe–Cu@PVP adsorption, and the Fenton oxidation during the CIP removal process revealed that the Fe–Cu@PVP adsorption and Fenton oxidation dynamically evolved throughout the removal process, with Fenton oxidation significantly increased as the process advanced (Fig. 12).[169]

Enrofloxacin, marketed as Baytril and other brands, is a fluoroquinolone antibiotic for animals, exerting bactericidal effects. Its activity is concentration-dependent, leading to susceptible bacteria's demise within 20–30 min of exposure.[170] The United States banned enrofloxacin for poultry in 2005 due to its association with the emergence of fluoroquinolone-resistant strains of Campylobacter, a human pathogen.[171] Yu *et al.* synthesized metal–organic frameworks (MOFs) and utilized as precursors to fabricate iron-based heterogeneous Fenton catalysts, namely Fe@C, Fe–Cu@C, and Fe–Cu@N–C, through pyrolysis. The assessment of catalytic efficacy was conducted by quantifying the hydrogen peroxide (H_2O_2) decomposition rate. The experimental studies revealed that after 60 min, the Fe–Cu@C and Fe–Cu@N–C mediated decomposition rates of H_2O_2 were 95.4% and 92.5%, respectively, significantly higher than those by Fe@C by 18.5% and 15.6%. This enhancement was ascribed to the presence of iron and copper species within the bimetallic nanoparticles, serving as active sites for the Fenton reaction. The synergistic effects between these elements were responsible for inducing the activation and breakdown of H_2O_2. Additionally, the N-doped catalysts, Fe–Cu@N–C, exhibited superior pH adaptability, reusability, and reduced iron leaching compared to Fe–Cu@C. The enhanced catalytic performance of bimetallic nanoparticles was attributed to the well-dispersed nature of Fe and Cu species on the nitrogen-doped carbon matrix. Further, the efficacy of Fe–Cu@N–C was also tested for degradation of enrofloxacin (ENR) antibiotics in wastewater. The results indicated a 90% degradation rate within 60 min under the following conditions: initial ENR concentration of 20 mg L^{-1}, catalyst dosage of 20 mg L^{-1}, H_2O_2 concentration of 1.5 mM, initial solution pH of 3.6, and temperature of 25 °C. The rapid degradation of ENR was mainly ascribed to surface-bound $^{\bullet}OH$ radicals rather than free $^{\bullet}OH$ plays the dominant role, generated from heterogeneous Fenton reactions.[172]

Ofloxacin, a fluoroquinolone antimicrobial, treats diverse bacterial infections, including pneumonia, cellulitis, urinary tract infections, and prostatitis. Zheng *et al.* explored the heterogeneous Fenton-like degradation of ofloxacin (OFL) employing the synergistic degradation approach of bimetallic Fe–Cu nanoparticles supported on the ordered mesoporous silicon (Fe–Cu@MPSi). The characterization techniques including XRD, TEM, SEM, and N_2 sorption–desorption isotherms revealed that Fe–Cu@MPSi exhibits an ordered mesoporous structure with high BET surface area, uniform mesopore size (~2.4 nm), and moderate pore volume (0.19 cm^3 g^{-1}). The Fe_2O_3 and CuO nanoparticles were observed to be highly dispersed within the mesopore channels and on the surface of the catalyst. The degradation mechanism of Fe–Cu@MPSi was investigated under optimal oxidation conditions of 30 mg L^{-1} OFL, 1 g L^{-1} of catalyst dose, 2000 mg L^{-1} of H_2O_2, and initial pH. By using the enhanced mass and electron transfer properties of mesoporous silicon, as well as the synergistic interfacial effect of Fe and Cu on the catalyst surface, and the complexation of OFL with Cu^{2+}, the Fe–Cu@MPSi composite displayed exceptional and selective degradation of OFL.[173]

Stavudine and Zidovudine, are a class of medications called nucleoside reverse transcriptase inhibitors (NRTIs) and is an antiretroviral medication used to prevent and treat HIV/AIDS.[174] The antiviral medications might have diverse harmful impacts on non-target aquatic organisms across various trophic levels. Ayodhya *et al.* introduced a novel method for the synthesis of bio-functionalized bimetallic nanoparticles (BMNPs) of silver–gold (Ag–Au@Chry), silver–copper (Ag–Cu@Chry), and gold–copper (Au–Cu@Chry) using Chry as a bio-reductant and as a capping agent. Chry is a natural anticancer bioflavonoid with a huge potential for cancer treatment. The BMNPs were tested for the catalytic degradation of HIV drugs stavudine (STV) and zidovudine (ZDV)) in the presence of $NaBH_4$ as a reducing agent in an aqueous medium. The Ag–Au@Chry BMNPs exhibited the highest degradation efficiency (approximately 96%) for STV and ZDV within 18 min of reaction time and also maintained the catalytic activity throughout the five consecutive runs. The antimicrobial activity of the synthesized BMNPs (20 μg mL^{-1}) was also evaluated against *Escherichia coli*, *Pseudomonas aeruginosa, Staphylococcus aureus*, *Bacillus subtilis* bacteria, as well as fungi including *Aspergillus niger* and *Candida albicans* using the well diffusion method.[175]

Cyclophosphamide, also called cytophosphane, is a drug employed in chemotherapy and immune system suppression. It treats various cancers like lymphoma and leukemia. However, after its bioactivation to alkylating metabolites, it becomes

carcinogenic through a genotoxic mechanism.[176] Pérez-Poyatos *et al.* synthesized bimetallic (Fe–Cu) and reduced graphene oxide Fe–Cu@rGO catalysts at 0.2% wt. using a co-precipitation method, varying Fe–Cu molar ratios (40 : 60, 20 : 80, and 10 : 90), and evaluating their efficacy in degrading the cytostatic drug cyclophosphamide (CP) in water through a UV-Vis assisted photo-Fenton process. The physicochemical analysis *via* gas adsorption, SEM, TEM, XRD, and XPS analysis was conducted to correlate results with the catalytic performance. The pH influence on contaminant degradation and catalyst stability (metal leaching) were also examined. The results explained the synergistic effect of Fe–Cu@rGO catalysts compared to monometallic counterparts or those lacking carbonaceous material in degrading CP. The Fe–Cu@rGO (10 : 90) catalyst exhibited the highest performance, degrading nearly 82% of CP at natural pH and 87% at pH 3, diminishing the need for acidification during the Fenton-like processes and minimizing metal leaching, with increased catalyst stability maintained above 75% efficiency observed in consecutive degradation cycles.[177]

Sulfathiazole is a short-acting sulfa drug. It used to be a common oral and topical antimicrobial. Its eco-toxic effects include a significant negative impact on soil.[178] Niu and colleagues developed a ternary micro-electrolysis setup comprising of carbon-coated metallic iron with Cu nanoparticles (Fe^0–C@Cu^0) to degrade sulfathiazole (STZ). These catalysts showed exceptional reusability and stability due to the tailored Fe^0 with persistent activity. When compared to the catalysts prepared with $FeSO_4 \cdot 7H_2O$ and iron(II) oxalate, those synthesized with iron citrate demonstrated a stronger Fe–Cu connection. The carbon layer facilitated the electron transfer from Fe^0 to Cu^0, thus promoting the STZ degradation. Further, the high potential difference between the cathode (C and Cu^0) and anode (Fe^0) accelerated Fe^0 corrosion enhancing STZ degradation *via* a Fenton-like process. The core–shell structure of the Fe^0–C@Cu^0 catalyst exhibits enhanced STZ degradation with a two-stage reaction driven by the synergistic effects of Fe^0–C@Cu^0. Further, the Fe^0–C@Cu^0 catalysts exhibit excellent performance for sulfathiazole degradation in landfill leachate effluent.[179]

Tetracycline, an oral antibiotic, treats infections like acne, cholera, and malaria. It can alter bacterial activity in water, and potentially have a negative effect on the aquatic ecosystem upon entry.[37] SefidSiahbandi *et al.* evaluated the use of a novel adsorbent HEC-GO comprising biodegradable hydroxyethylcellulose (HEC) and graphene oxide (GO), crosslinked with ethylene glycol dimethacrylate (EGDMA). The HEC-GO was used as a support for Fe–Zn bimetallic nanoparticles at a mole ratio of 1 : 1, and was used for the removal studies of tetracycline (TC). The results revealed that HEC-GO and HEC-GO/Fe–Zn (1 : 1 mole ratio) nanocomposites exhibited high adsorption capacities for TC, particularly at pH 3, with optimal contact times of 100 and 20 min, respectively. The TC removal percentages were 85% and 95% for HEC-GO and HEC-GO/Fe–Zn, respectively. The isotherm models, particularly the Langmuir model described the maximum adsorption capacity for TC and the kinetic studies explained that TC adsorption on HEC-GO and HEC–GO/Fe–Zn (1 : 1 mole ratio) followed the pseudo-second-order kinetic model. Thermodynamic analysis suggested that the adsorption process was spontaneous and exothermic.[180] Kaushal *et al.* used precipitation refluxing method to synthesize Zr/Cu-MOF used for the photocatalytic removal of tetracycline. The Zr/Cu-MOF exhibited remarkable effectiveness in breaking down tetracycline, achieving a degradation efficiency of 93% within 80 min. Analysis of radical scavenging indicated that hydroxyl radicals ($^{\bullet}OH$) play a crucial role in the photocatalytic decomposition process. To predict intermediates and propose the degradation mechanism of tetracycline, liquid chromatography-mass spectrometry (LC-MS) analyses were conducted.[181] Musa *et al.* introduced cobalt oxide/iron oxide bimetallic nanoparticles (Co_3O_4–Fe_3O_4 NPs) using a chemical coprecipitation method. The characterization using SEM and XRD revealed plate-like structures of Co_3O_4–Fe_3O_4 NPs, which were agglomerated as irregular spheres with size of 101.85 nm. These NPs were found effective in adsorbing Tetracycline (TC) from aqueous solutions, with optimal conditions at pH 9.0, and an adsorbent concentration of 3.0 g L^{-1}. The Langmuir isotherm model was observed as best fit for the experimental data, showing a maximum monolayer adsorption capacity of 149.26 mg g^{-1} at 55 °C. The kinetic data was well aligned with the pseudo-second-order model, and the mass transfer modeling indicated both film and intra-particle diffusion played a significant role in the TC removal process. The thermodynamic analysis suggested an endothermic, spontaneous process with an increased disorderness at the solid–solution interface exhibiting a positive ΔS value. Moreover, the adsorbent maintained a high efficiency of TC removal over seven consecutive uses.[182] Gopal *et al.* utilized the nano zero-valent technology for antibiotic remediation, employing bimetallic Fe–Cu nanoparticles synthesized with pomegranate rind extract. They achieved a 72 ± 0.5% removal of TC (10 mg L^{-1}) with Fe–Cu nanoparticles (750 mg L^{-1}) at pH 7. Further, to address the colloidal instability and to enhance the TC removal, the bimetallic nanoparticles were synthesized *in situ* on the bentonite support, creating (Fe–Cu@B) composite. The treatment with Fe–Cu@B at pH 7 and a concentration of 150 mg L^{-1} resulted in a remarkable removal of 95 ± 0.05% of TC, demonstrating a significant enhancement with a reduced nanoparticle loading. The removal process was monitored using UV-Vis analysis along with total organic carbon (TOC), oxidation–reduction potential (ORP), and liquid chromatography-mass spectrometry (LCMS) measurements. The composite exhibits significant stability even after three cycles of operation, and the validation was also conducted in real water systems.[183]

Doxycycline is a broad-spectrum antibiotic used to treat infections caused by bacteria and parasites. It is also used to treat bacterial pneumonia, chlamydia infections, acne, Lyme disease, typhus, cholera, and syphilis. It is also used to prevent malaria. However, Doxycycline has negative ecotoxicological impacts.[184] SefidSiahbandi *et al.* conducted research to fabricate the hydroxyethyl cellulose-graphene oxide (HEC-GO) and Fe–Zn@HEC-GO nanocomposites with a mole ratio of 2 : 1, utilizing cross-linked ethylene glycol dimethacrylate (EGDMA) as the crosslinking agent. The study aims to investigate the

thermodynamic, kinetic, and isotherm aspects of doxycycline antibiotic adsorption. The optimal conditions for DOX removal were determined as pH = 3.0, with contact times of 100 min and 20 min HEC-GO and Fe–Zn@HEC-GO, respectively. The removal percentages for HEC-GO and Fe–Zn@HEC-GO were 97% and 95.5%, respectively. The equilibrium adsorption isotherms, including Langmuir, Freundlich, and Temkin models, were analyzed for their best fit of experimental data, however, the Langmuir isotherm was proved to be the best in experimental findings. Among the four-adsorption kinetics investigated for DOX removal, the pseudo-second-order (PSO) kinetic models provided the best fit for experimental data for HEC-GO and Fe–Zn@HEC-GO. The thermodynamic data indicated the negative values of Gibbs free energy (ΔG°) and enthalpy (ΔH°) for the adsorption process, suggesting a spontaneous and exothermic reaction for DOX removal by HEC-GO and Fe–Zn@HEC-GO composite.[185]

Chlortetracycline, a tetracycline antibiotic, treats conjunctivitis in cats, dogs, and horses, and infected wounds in cattle, sheep, and pigs. Its transmission across generations can compromise offspring immune defenses, raising concerns about antibiotic's population risks in the environment.[186] Xia and colleagues developed a novel bimetallic metal–organic gel (JLUE-MOG-Fe/Y) using a solvothermal method, and utilized it for the adsorptive removal of chlortetracycline hydrochloride (CTC) from aqueous solutions. The JLUE-MOG-Fe/Y exhibited remarkable stability, broad adaptability, and excellent recyclability, with a robust CTC adsorption capacity of up to 584.83 mg g^{-1} at 25 °C. The adsorption process of CTC on the JLUE-MOG-Fe/Y was found to be exothermic and spontaneous, and the adsorption data was fitting well with the pseudo-second-order kinetic model and Freundlich isotherm model. The adsorption experiments and characterization results revealed that pore filling, coordination bonds, electrostatic interactions, π–π interactions, hydrogen bonds, and hydrophilic/hydrophobic interactions all contributed to the adsorption process[187] (Fig. 13).

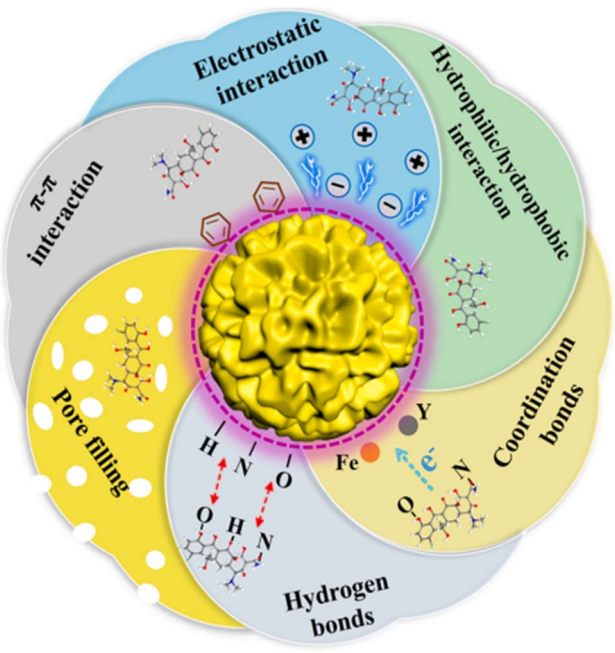

Fig. 13 The possible mechanism of chlortetracycline hydrochloride adsorption on JLUE-MOG-Fe/Y[187] (reproduced with permission, Elsevier, 2022).

Oxytetracycline disrupts bacteria's protein production, inhibiting growth. Its refractory nature, compounded by aquifer media of varied particle sizes, hampers O_3-pollutant contact, reducing oxidation efficiency.[188] Jin *et al.* investigated a nano-sized iron/nickel (Fe–Ni) functionalized zeolitic imidazolate framework-8 (Fe–Ni@ZIF-8) designed for oxytetracycline (OTC) removal from wastewater. The results from cyclic voltammetry and amperometric *I–t* measurements suggested that OTC degradation occurred with Fe–Ni@ZIF-8. The structural analysis through X-ray diffraction spectroscopy (XRD), transmission electron microscopy mapping (TEM-mapping), and X-ray photoelectron spectroscopy (XPS) revealed a uniform dispersion of Fe–Ni throughout the ZIF-8 framework, with a partial oxidation observed in post-reaction with OTC. The OTC adsorption isotherms and kinetics were best described by the Langmuir isotherm (R^2 > 0.982), and pseudo-second-order model (R^2 > 0.997), respectively. The reduction kinetics data followed the pseudo-first-order model (R^2 > 0.905), with an apparent activation energy (E_a) value of 22.9 kJ mol^{-1}, indicating the chemical degradation of OTC. In practical applications, Fe–Ni@ZIF-8 exhibited a removal efficiency of 92.6% for OTC from real wastewater. The Fe–Ni@ZIF-8 maintained a high removal rate of 74.9% even after 5 consecutive OTC removal cycles, highlighting its good efficacy and recyclability[189] (Fig. 14).

Nguyen *et al.* conducted a study on the reduced graphene oxide-supported bimetallic palladium-zero-valent-iron (Pd–Fe@rGO) composites, synthesized using a one-step liquid-phase reduction method. The synthesized Pd–Fe@rGO composites were utilized for oxytetracycline (OTC) removal from aqueous solutions. The transmission electron microscopy (TEM) and X-ray diffractometry (XRD) analysis revealed that rGO sheets prevented Pd–Fe bimetallic nanoparticle aggregation resulting in more homogeneous dispersion of nanoparticles, and thus delayed the formation of iron corrosion products. Moreover, Pd–Fe bimetallic nanoparticle loading effectively prevented the rGO sheet stacking. The addition of an optimal amount of rGO significantly enhanced the OTC removal, with 5 wt% rGO in Pd–Fe@rGO composite (dose, 0.1 g L^{-1}) achieved the highest removal efficiency of 96.5% (OTC initial concentration: 100 mg L^{-1}) after a 60 min reaction at pH 5.0 and 25 °C. OTC removal by Pd–Fe@rGO composite involved the combination of the adsorption, Fenton-like reactions, and reduction processes for the OTC removal. The composites exhibited superior reusability compared to pristine nano zero-valent-iron (nZVI particles).[190]

Sulfamethazine, a sulfonamide, features pyrimidine with methyl groups at 4- and 6-positions and a 4-amino-benzenesulfonamido group at the 2-position. It acts as an antiinfective, antibacterial, and antimicrobial agent, treating infections like bronchitis and prostatitis. Residual

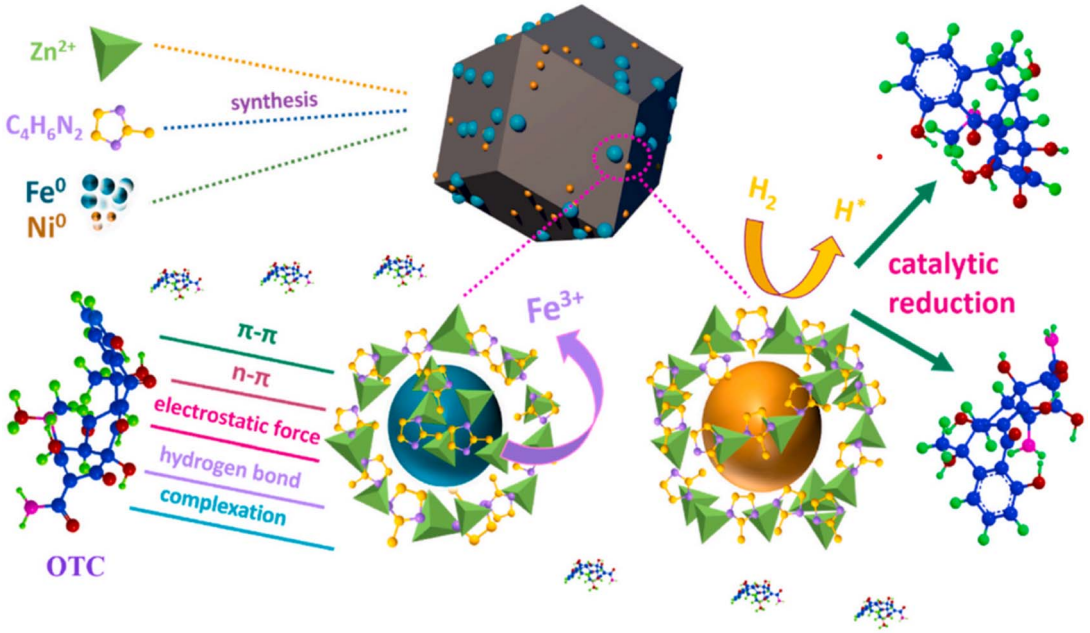

Fig. 14 Proposed mechanism of oxytetracycline removal by Fe–Ni@ZIF-8 (Jin *et al.*, 2022) (reproduced with permission, Elsevier, 2022).

sulfamethazine may persist due to its stability in certain environments, as evidenced by studies showing its presence in groundwater and soil for over 60 days post-application.[191] Dong *et al.* synthesized the zero-valent Fe–Cu bimetallic nanoparticles through a straightforward method and used these bimetallic nanoparticles to activate sulfite for sulfamethazine (SMT) degradation in aqueous solutions. The key factors affecting SMT degradation, including the theoretical loading of Cu, Fe–Cu catalyst dosage, sulfite concentration, and initial solution pH were systematically investigated and revealed that the Fe–Cu/sulfite system outperformed the bare Fe^0/sulfite system in SMT degradation. The study revealed that the Cu loading induced synergistic effects between Fe and Cu, and affects the potential degradation pathway of SMT in the Fe–Cu/sulfite system, which involve hydroxyl ($^{\bullet}OH$) and sulfate ($SO_4^{\bullet-}$) radicals as the primary reactive radicals. The redox cycle between Cu(I)/Cu(II) significantly facilitated the conversion of Fe(III) to Fe(II), and thus enhanced the catalytic performance of the Fe–Cu bimetallic nanoparticles. The catalyst's stability and reusability was evidenced through the aging tests conducted over a period of 30 days on Fe–Cu particles and recycling experiments, which indicated a minimal impact on SMT removal by Fe–Cu bimetallic nanoparticles.[192]

Mahlaule-Glory *et al.* performed a study where bimetallic ZnO–SnO_2 nanoparticles were synthesized using *Sutherlandia frutescens* plant extract and were evaluated for their effectiveness in degrading the methylene blue (MB) dye, sulfisoxazole (SSX), and sulfamethoxazole (SMX) antibiotics. The SEM imaging suggested the homogeneous and heterogeneous structures consisting of tubular and spherical shapes, with the particle sizes ranging from 5 to 60 nm. The XRD analysis confirmed the crystallinity of the nanoparticles. The UV-Vis spectroscopy determined the optical properties, with band gap values ranging from 3.08 to 3.3 eV. The surface area analysis indicated type III isotherms and mesoporous structures for the bimetallic nanoparticles. The assessment of photocatalytic activity of these nanoparticles for MB dye, SSX, and SMX antibiotics suggested that the 50 : 50 loading ratio exhibited the highest MB degradation of 88% within 150 min, with a rapid kinetic rate of 0.0008 min^{-1}, whereas, the SSX and SMX antibiotics showed degradation rates of 66% and 70%, respectively.[193]

Naproxen and Diclofenac, nonsteroidal anti-inflammatory drugs (NSAIDs), alleviate mild-to-moderate pain and arthritis symptoms by reducing inflammation, swelling, stiffness, and joint pain. These are detected in various waters and their low concentrations may adversely affect nontarget organisms with prolonged exposure.[194] Sahin *et al.* employed *Lathyrus brachypterus* extract to synthesize magnetic iron oxide and iron-copper nanoparticles. Subsequently, they synthesized magnetic Fe_3O_4@CS, Fe_3O_4@AT, Fe–Cu@CS, and Fe–Cu@AT nanocomposite beads using chitosan (CS) and alginate (AT) natural polymers. These materials served as both adsorbents and heterogeneous catalysts for the catalytic wet peroxidation (CWPO) of naproxen (NPX), diclofenac (DCF), and the combination of NPX and DCF, from aqueous medium. In adsorption studies, the rapid drug adsorption occurred within min followed by desorption between 8 and 10 min. During the competitive adsorption, the adsorbents exhibited selectivity towards DCF and NPX. In CWPO, the drug removal reached 92% conversion for DCF and 84% for NPX within 9 min under optimum conditions *i.e.* pH 5, 30% H_2O_2, catalyst dose of 100 mg, and 298 K, with Fe–Cu@CS and Fe–Cu@AT catalysts, respectively, showing the best performance. The reusability tests indicated a slight decrease in removal efficiencies by the third cycle, however, the catalysts maintained their stabilities

and active structures. Further, the oxidation reaction conformed well to the pseudo-first-order kinetic model.[195] He *et al.* developed an Iron/copper bimetallic nanoparticles-supported on the sludge biochar (Fe–Cu@SBC) *via* a modified co-precipitation method. The Fe–Cu@SBC system was utilized to activate periodate (IO_4^-) for diclofenac sodium (DCF) degradation under the UV light at 25 °C. The physicochemical characteristics of both SBC and Fe–Cu@SBC, including morphology, crystal structures, and the surface functional groups, suggested that while the modification with Fe–Cu bimetallic nanoparticles the surface functional groups increased and thus resulted in enhanced catalytic performance. The various parameters affecting catalytic efficiency were investigated and optimized including periodate concentration (5 mM), catalyst dosage (0.1 g), UV power (60 W), and initial pH 6.9. Under optimal conditions, the DCF degradation of 99.7% was observed with a pseudo-first-order kinetics reaction constant of 9.39×10^{-2} min^{-1}. The radical scavenging experiments revealed $IO_3^{\bullet}$ radicals as the primary reactive oxidants in the Fe–Cu@SBC/UV system.[196] Ghauch *et al.* evaluated the aqueous removal of diclofenac (DF) using micrometric iron particles (Fe^0) and modified Fe^0–M^0@Fe^0 under both oxic and anoxic conditions. Bimetallic systems were created by coating the surface of Fe^0 with M = Co, Cu, Ir, Ni, Pd, and Sn. The experimental findings explained the superior performance of M^0@Fe for DF removal, except for Ir@Fe (oxic) and Sn@Fe (anoxic) systems. Under anoxic conditions, Pd exhibited the highest efficiency among the plating elements, followed by Ir, Ni, Cu, Co, and Sn. On the other hand, under oxic conditions, Pd and Cu displayed nearly equal efficiency in DF removal, followed by Ni, Co, Sn, and Ir. The oxidative and reductive transformation products of DF were identified under oxic and anoxic conditions, respectively. In certain systems (*e.g.*, Co@Fe and Sn@Fe under both oxic and anoxic conditions; Pd@Fe under oxic conditions; Ni@Fe under anoxic conditions), no transformation products were observed. This was attributed to the nature of the plating element and its influence on the formation process of metal corrosion products (MCPs). The MCPs are recognized for their ability to strongly adsorb, bind, and encapsulate both the original contaminant and its reaction products. These results support the general impression that the aqueous contaminants are primarily removed through adsorption and co-precipitation processes.[197]

Pan *et al.* introduced a facile self-adjusted strategy (SAS) to develop bimetallic zeolitic-imidazolate framework (Co_xZn_y-JUC-160) for synthesizing various N-doped Co-based hierarchical porous carbon composites (Co@NC) *via* a sacrificial template route. This synthetic strategy provides valuable insights into developing highly efficient, recyclable magnetic adsorbents for contaminant removal. The highly porous magnetic materials with finely tuned Co and Zn ratios in the precursors resulted in well-dispersed or reduced Co particle sizes. The optimal Co@NC composite exhibited a large specific surface area, hierarchical pore structures, and a well-distributed Co adsorption sites, facilitating the exposure of active Co centers and rapid diffusion of amodiaquine (ADQ) molecules with a record-high adsorption capacity of 890.23 mg g^{-1}. The study systematically investigated the effect of Co–Zn ratios on the textural properties and drug adsorption performance of the resulting porous carbon composites.[198]

Amoxicillin, an antibiotic in the aminopenicillin class, treats bacterial infections like middle ear, strep throat, and urinary tract infections. It can affect microorganism operative in wastewater treatment and promote bacterial resistance.[199] Wen *et al.* introduced a synthesis approach for a novel coordinatively unsaturated cobalt–iron (Co–Fe) bimetallic metal–organic frameworks (MOFs) as a heterogeneous catalyst for the Fenton-like process in the degradation of amoxicillin (AMX), in the presence of H_2O_2. To optimize the process, the effects of catalyst dosages, H_2O_2 concentrations, initial pH, and the coexisting anions on AMX degradation was determined. The results revealed a complete AMX degradation at pH 7, with H_2O_2 concentration of 3 mM, and a catalyst dose of 0.1 g L^{-1}. It was observed that even after five cycles of reusability, the coordinatively unsaturated cobalt–iron bimetallic MOFs retained a substantial Fenton-like catalytic activity (achieving 100% degradation within 30 min). Further, the synthesized cobalt–iron-based MOFs with coordinated sites exhibited significant antibacterial efficacy in disc diffusion analysis.[200] Zhang *et al.* utilized carbon nanofibers supported with Co–Ag bimetallic nanoparticles (Co@CNFs–Ag) to activate peroxymonosulfate for the heterogeneous Fenton-like process to efficiently oxidize amoxicillin (AMX). To minimize the loss of Co during the preparation and catalysis steps, the Co nanoparticles (20–30 nm) were encapsulated within the carbon nanofibers, while Ag nanoparticles (5–10 nm) were distributed on the CNFs' surface. The study elucidated the reaction mechanism of the bimetallic synergistic catalytic system and potential amoxicillin degradation pathways, offering valuable insights for employing sulfate radical-based advanced oxidation processes in environmental cleanup. The Co@CNFs–Ag activated peroxymonosulfate system achieved complete removal of amoxicillin within 30 min. This high catalytic efficiency originated from the carbon nanofibers' large aspect ratio (>10 000) and the synergistic interaction between the Co–Ag bimetallic nanoparticles and peroxymonosulfate. The optimal mass ratio of oxidant to catalyst was 10, with pH 7 being the optimized condition. The Co@CNFs–Ag composite demonstrated the stable catalytic activity and minimal metal leaching over 5 cycles, with an activation energy of 29.51 kJ mol^{-1} calculated using the Arrhenius equation. It was the both hydroxyl and sulfate radicals that contributed to amoxicillin degradation, with the latter being the main contributing factor[201] (Fig. 15).

Yazdanbakhsh *et al.* evaluated the degradation of amoxicillin trihydrate (AMT), using the synthesized nanoscale zero-valent iron (nZVI) and bimetallic Fe–Ni nanoparticles stabilized on chitosan (Fe–Ni@Cs). A central composite design combined with response surface methodology (RSM) and optimization was employed for maximizing the AMT reduction using nanoparticles–water system. Field-emission scanning electron microscopy images indicated that the chitosan acts as a stabilizer and prevents the agglomeration of nanoparticles. Further, the chitosan and Ni increased the specific surface area of Fe–Ni@Cs. The effects of independent parameters were evaluated and the results showed that the initial concentration of AMT,

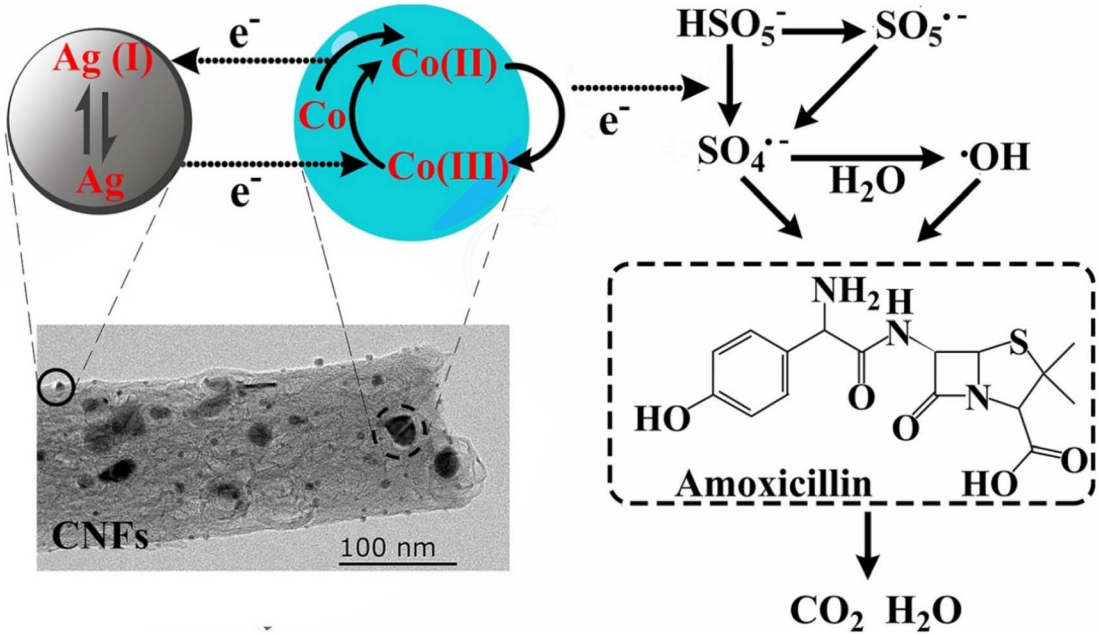

Fig. 15 Removal of amoxicillin using Co@CNFs–Ag bimetallic nanocomposite for heterogeneous activation of peroxymonosulfate[201] (reproduced with permission, Elsevier, 2020).

pH, and nZVI or Fe–Ni bimetallic nanoparticles dosage, were all significant factors contributing to the removal of AMT. The X-ray diffraction (XRD) confirmed the presence of Fe^0 in the fresh samples and the presence of Fe(II) and Fe(III) after the reaction with AMT.[202]

Doxorubicin, marketed as Adriamycin, is a chemotherapy drug for breast cancer, lymphoma, and leukemia. It's used with other agents. Eco-genotoxicity studies found that at a concentration of 0.05 μg L^{-1}, it damages DNA in *Ceriodaphnia dubia* cells.[203] Fu *et al.* used the potential of iron and palladium doped graphite carbon nitride (g-C_3N_4@Fe–Pd) for investigating the removal performance, mechanism, and pathway in the removal of doxorubicin (DOX) from water. The structural analysis of g-C_3N_4@Fe/Pd revealed the decoration of the metallic Pd clusters on the surface of uniformly distributed iron nanoparticles (~28 nm) on the g-C_3N_4. The presence of g-C_3N_4 effectively decreased the agglomeration and overgrowth of the iron nanoparticles, while the strong coupling effect among Fe, Pd, and N displayed excellent DOX removal performance (k = 0.115 min^{-1}), demonstrating the versatility across the different initial concentrations (30–150 mg L^{-1}) and material dosages (0.1–0.4 g L^{-1}). Among the three potential degradation pathways for DOX proposed, the catalytic saccharide moiety elimination was identified as the primary route. The intermediates displayed reduced toxicity, and the final degradation product was efficiently adsorbed by g-C_3N_4@Fe/Pd.[204] Kadu *et al.* investigated the degradation of doxorubicin (DOX), a widely recognized anticancer agent, using Fe–Ni bimetallic nanoparticles (Fe–Ni NPs). These nanoparticles degraded the DOX through a chemisorptive, exothermic, and pseudo-multilayer film-diffusion mineralization process, as evidenced by the adsorption and intra-particle mechanisms. The liquid chromatography-mass spectrometric (LC-MS) analysis of metabolites formed during the degradation helped in establishing the degradation mechanism (Fig. 16), which closely resembled the metabolic pathway mediated by aldo–keto reductase (AKR), an oxido-reductase enzyme family involving the reactive oxygen species (ROS) and the iron–sulfur clusters. The XPS analysis indicated the formation of an oxide layer on the nanoparticle surface, reducing their recycling capacity. The toxicity evaluation of the degraded DOX solution against two breast cancer cell lines, MCF-7 and MDA-MB-231, and a normal cell line, HEK-293, revealed the non-toxic nature of the metabolites. The chemo-informatic studies performed using the Molinspiration Properties Calculator (MPC) supported these findings. Thus, Fe–Ni NPs exhibit properties akin to a functional mimic of AKR, facilitating eco-friendly DOX degradation.[205]

Metformin, marketed as Glucophage, is a first-line medication for type 2 diabetes and polycystic ovary syndrome. It is a biguanide drug, that lowers blood glucose by decreasing production, and absorption, and enhancing insulin sensitivity. It is detected in surface water at concentrations ranging from ng L^{-1} to μg L^{-1}, however, its eco-toxic impacts are poorly studied.[206] Abd El-Aziz *et al.* successfully utilized a green synthesis approach employing *Ficus benjamina* leaves extract to synthesize the bimetallic zero-valent iron/copper (Fe–Cu) nanoparticles and were used for the removal of metformin HCl (MF) from aqueous medium. The removal efficiency of metformin HCl (10 mg L^{-1}) reached 73% under conditions of pH 5, dosage of 0.2 g L^{-1}, and a reaction time of 30 min. The bimetallic Fe–Cu nanoparticles exhibited good durability, stability, and remarkable reusability for MF removal, even after five cycles of reuse. The Langmuir adsorption model provided a better fit with the isotherm data, showing high correlation coefficients

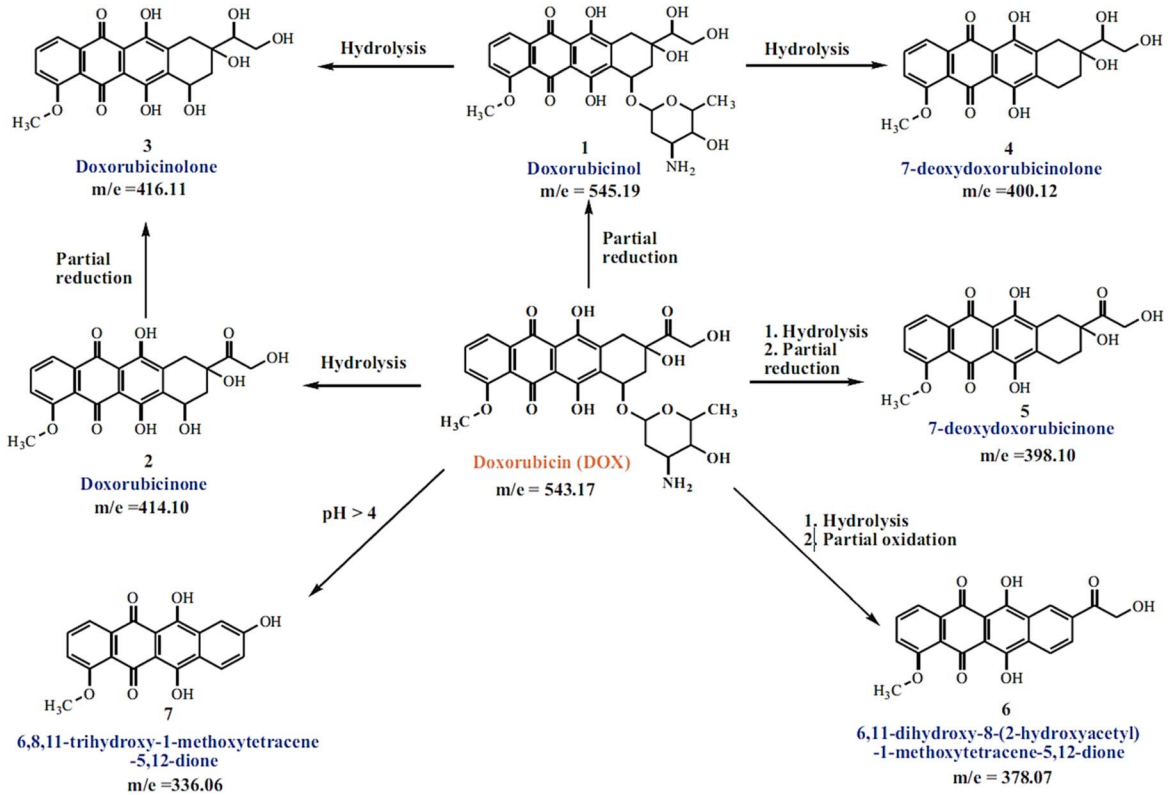

Fig. 16 HRMS analysis of formation of secondary metabolites from doxorubicin degradation with Fe–Ni NP's[205] (reproduced with permission, Elsevier, 2017).

(R^2 = 0.9991) with a maximum adsorption capacity (q_{max}) of 42.82 mg g^{-1}. The adsorption kinetics analysis revealed that MF uptake on *Ficus benjamina* using Fe–Cu nanoparticles followed the pseudo-second-order kinetic model. The study of operational parameter effects using SPSS linear regression analysis showed that these parameters had a significant impact of over 97% on the overall removal process.[207]

Nafcillin sodium, a narrow-spectrum beta-lactam antibiotic in the penicillin class, treats infections caused by Gram-positive bacteria, especially resistant staphylococci species. Campos *et al.* explored the heterogeneous electro-Fenton (HEF) as an alternative to conventional electro-Fenton (EF), where HEF utilizes a solid phase catalyst compared to EF's solubilized one. This distinction allows for an easy material recovery in HEF through simple separation methods like filtration or magnetic separation. Moreover, the HEF eliminates the need for prior pH adjustment, thus enabling the operations within a broader pH range. In their study, they synthesized, characterized, and utilized Fe, Cu, and Fe–Cu bimetallic nanoparticles (Fe–Cu NPs) for degrading Nafcillin (NAF). The effects of adsorption and anodic oxidation (AO-H_2O_2) processes on HEF were investigated. The NAF adsorption alone resulted in a modest antibiotic removal of up to 24%, while the AO-H_2O_2 process achieved a complete NAF removal after 240 min of electrolysis. It was evident that by using Fe–Cu NPs in the HEF process, a complete NAF elimination was achieved within a 7 min of electrolysis, with mineralization reaching up to 41% after 240 min. The NAF degradation was mainly observed due to hydroxyl radical generation on the boron-doped diamond (BDD) electrode as a result of Fenton reaction with Fe and Cu NPs. Further, the HEF successfully eliminated the antibiotic from slaughterhouse wastewater within 15 min of treatment using Fe–Cu bimetallic NPs.[208]

Carbamazepine is an anticonvulsant medication for epilepsy and neuropathic pain. Abd El-Aziz and coworkers produced eco-friendly synthesized bimetallic nano zero-valent Fe/Cu utilizing leaves of *Ficus Benjamina* (FB@Fe/Cu). These nanoscale zero-valent Fe/Cu particles were employed for the elimination of carbamazepine from the aqueous solutions, achieving 95% removal efficiency with a dose of 0.4 g L^{-1}, a duration of 20 min, and a pH of 5. The analysis confirmed the formation of iron-copper bimetallic nanoparticles capped with biomolecules from leaves extract serving as stabilizing agent. The analysis of the removal data was conducted using Freundlich and Langmuir adsorption isotherms, with the Langmuir model (R^2 = 0.998) found to best fit the adsorption data, yielding a maximum adsorption capacity (q_{max}) of 26.15 mg g^{-1}.[209]

Triclosan, found in various consumer products like toothpaste and soaps, acts as an antibacterial and antifungal agent, similar to triclocarban. Its lipophilicity and bioaccumulation pose risks to ecosystems and human health.[210] Lin *et al.* conducted green synthesis of bimetallic iron–nickel nanoparticles (Fe–Ni NPs) for the simultaneous removal of triclosan (TCS), an antibacterial and antifungal agent, and Cu(II) from aqueous

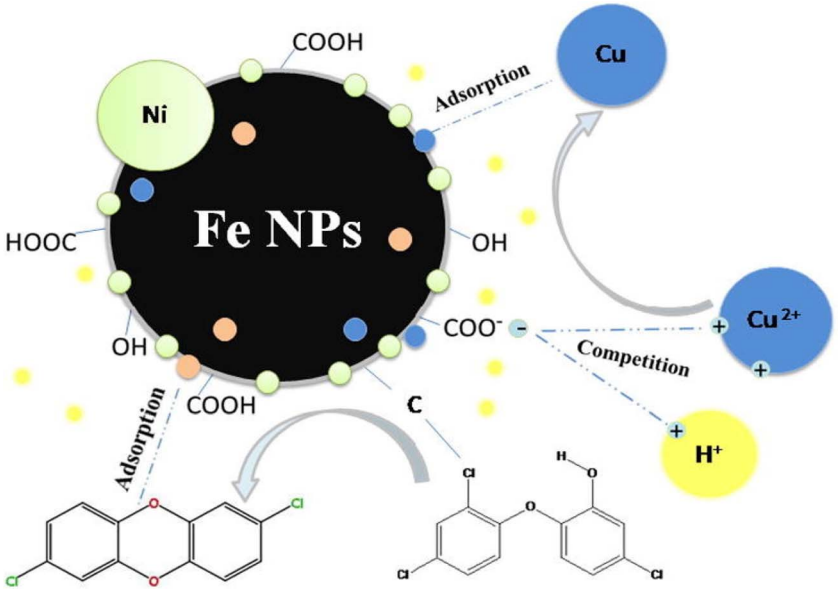

Fig. 17 Removal of triclosan using Fe–Ni NPs[211] (reproduced with permission, Elsevier, 2019).

medium. With the Fe–Ni bimetallic system, the TCS and Cu(II) removal efficiencies were 75.8% and 44.1%, respectively, under optimal conditions. In a mixed contaminant system, the removal efficiencies were lower (TCS: 85.8%, Cu(II): 52.5%), indicating a competition between contaminants and Fe–Ni NPs. The analysis techniques (SEM-EDS, XRD, FTIR, XPS, GC-MS) confirmed the adsorption and reduction of TCS and Cu(II) on Fe/Ni NPs surface. The kinetic models and isotherms also revealed the adsorption and reduction mechanisms[211] (Fig. 17).

Gao and colleagues utilized *Ginkgo biloba* L. leaf extract to synthesize Fe–Co bimetallic nanoparticles (G–Fe–Co NPs) for TCS removal from water. The characterization *via* various techniques revealed the improved dispersion and reduced passivation of NPs. The TCS removal efficiency in decreasing order with various nanoparticle systems is as follows: G–Fe–Co NPs > G–Fe NPs > Co NPs > Fe–Co NPs > Fe NPs. The NPs could be reused up to eight times, with insignificant Co leaching at different initial pH values. When the factors influencing the TCS removal were investigated, the removal rate constant was observed to be decreased with increased initial pH and TCS concentration, and decreased Co loading and NPs dosage and followed pseudo-second-order kinetics. The mass balance indicated the adsorption as the dominant process, with TCS degradation as a cumulative process.[212]

7. Summary, challenges, and future prospective

This review provides an overview of the synthesis of bimetallic nanoparticles using both conventional and green methods, emphasizing their morphological characteristics, multifunctional properties, and broad applications. Bimetallic nanoparticles are gaining more attention than monometallic nanoparticles due to their superior catalytic performance, which results from the synergistic effects of combining two metals. This makes them particularly attractive for catalytic applications, such as the removal of Pharmaceuticals and Personal Care Products (PPCPs) from wastewater, due to their large surface area and enhanced reactivity. The review covers the preparation techniques of bimetallic nanoparticles, their catalytic mechanisms for PPCP degradation, and factors influencing catalytic efficiency, such as nanoparticle size, composition, and surface functionalization.

However, the development of bimetallic nanoparticles for PPCP remediation faces several challenges, including the need for precise control over synthesis, maintaining stability, ensuring selectivity, and addressing scalability. Achieving reproducible synthesis while controlling particle size, shape, and composition, and preventing agglomeration or degradation under environmental conditions, is crucial for optimizing their effectiveness. Furthermore, understanding the long-term environmental impacts and toxicity of these nanoparticles is essential for their safe deployment. Selectivity in targeting PPCPs within complex pollutant mixtures remains a challenge, but it is necessary for practical applications.

Scaling up bimetallic nanoparticle synthesis for industrial applications presents additional hurdles, such as the transition from laboratory-scale to large-scale production while maintaining the nanoparticles' desired properties. Issues related to the cost of raw materials, scalability of green synthesis methods, and ensuring consistency in nanoparticle quality across larger batches must be addressed for future real-world applications. Nevertheless, future advancements in bimetallic nanoparticle technology offer promising avenues, including improving reactivity through novel compositions and surface modifications, integrating nanoparticles with advanced treatment technologies, developing multifunctional systems, using advanced bio-inspired materials that can offer enhanced stability and

efficacy as capping agents, and establishing regulatory frameworks for safe use. These methods pave the way for more efficient and eco-friendly nanoparticle production, moving beyond current limitations.

By addressing these challenges, particularly in scaling up reactions for large-scale applications, and exploring the future directions for bimetallic nanoparticle technology, we can enhance their effectiveness in PPCP remediation and contribute to the protection of aquatic ecosystems and human health.

Data availability

The data that support the findings of this study are available from Royal Society of Chemistry, but restrictions apply to the availability of these data, which were used under license for the current study, and so are not publicly available. Data are however available from the authors upon reasonable request and with permission of Royal Society of Chemistry.

Author contributions

All authors have made significant contributions to the formulation and composition of this review article. Conceptualization: Sandeep Kumar, Sandeep Kaushal; methodology: Sandeep Kumar, Sandeep Kaushal, Ashish Singh Chauhan, Subbulakshmi Ganesan, Ashwani Kumar Sharma; validation: Subbulakshmi Ganesan, Ashwani Kumar Sharma, Ashish Singh Chauhan, Sandeep Kaushal, Sandeep Kumar; writing – original draft: Jyoti Rani, Tamanna Goyal, Arshdeep Kaur, Subbulakshmi Ganesan, Ashwani Kumar Sharma, Ashish Singh Chauhan, Sandeep Kaushal, Sandeep Kumar; writing – review & editing: Jyoti Rani, Subbulakshmi Ganesan, Ashwani Kumar Sharma, Ashish Singh Chauhan, Sandeep Kaushal, Sandeep Kumar; visualization: Jyoti Rani, Tamanna Goyal, Arshdeep Kaur, Subbulakshmi Ganesan, Ashwani Kumar Sharma, Ashish Singh Chauhan; supervision: Sandeep Kumar, Sandeep Kaushal.

Conflicts of interest

The authors declare no conflict of interest.

References

1 J.-L. Liu and M.-H. Wong, *Environ. Int.*, 2013, **59**, 208–224.
2 L. Yang, T. Wang, Y. Zhou, B. Shi, R. Bi and J. Meng, *Sci. Total Environ.*, 2021, **760**, 144080.
3 Y. Xiang, H. Wu, L. Li, M. Ren, H. Qie and A. Lin, *Ecotoxicol. Environ. Saf.*, 2021, **213**, 112044.
4 M. Kumar, B. Ram, R. Honda, C. Poopipattana, V. D. Canh, T. Chaminda and H. Furumai, *Sci. Total Environ.*, 2019, **693**, 133640.
5 X. Yuan, J. Hu, S. Li and M. Yu, *Environ. Pollut.*, 2020, **266**, 115340.
6 M. Alipour, H. Asadi, C. Chen and A. A. Besalatpour, *Fuel*, 2022, **319**, 123864.
7 X. Xin, G. Huang and B. Zhang, *J. Hazard. Mater.*, 2021, **410**, 124619.
8 P. Mathur, D. Sanyal, D. L. Callahan, X. A. Conlan and F. M. Pfeffer, *Environ. Pollut.*, 2021, **291**, 118233.
9 I. Virant-Klun, S. Imamovic-Kumalic and B. Pinter, *Antioxidants*, 2022, **11**, 1617.
10 R. Aimuzi, Y. Wang, K. Luo and Y. Jiang, *Chemosphere*, 2022, **302**, 134834.
11 K. Nozaki, R. Tanoue, T. Kunisue, N. M. Tue, S. Fujii, N. Sudo, T. Isobe, K. Nakayama, A. Sudaryanto, A. Subramanian, K. A. Bulbule, P. Parthasarathy, L. H. Tuyen, P. H. Viet, M. Kondo, S. Tanabe and K. Nomiyama, *Sci. Total Environ.*, 2023, **866**, 161258.
12 S. Keerthanan, C. Jayasinghe, J. K. Biswas and M. Vithanage, *Crit. Rev. Environ. Sci. Technol.*, 2021, **51**, 1221–1258.
13 M. Kumar, S. Sridharan, A. D. Sawarkar, A. Shakeel, P. Anerao, G. Mannina, P. Sharma and A. Pandey, *Sci. Total Environ.*, 2023, **859**, 160031.
14 I. Lozano, C. J. Pérez-Guzmán, A. Mora, J. Mahlknecht, C. L. Aguilar and P. Cervantes-Avilés, *Sci. Total Environ.*, 2022, **827**, 154348.
15 R. Y. Krishnan, S. Manikandan, R. Subbaiya, M. Biruntha, M. Govarthanan and N. Karmegam, *Environ. Technol. Innov.*, 2021, **23**, 101757.
16 S. Ghosh, B. Sarkar and S. Thongmee, in *Development in Wastewater Treatment Research and Processes*, Elsevier, 2024, pp. 149–166.
17 X. Ren, L. Shi, P. He, Y. Qian, Y. Wu, Z. Zhang and C. Gong, *Appl. Surf. Sci.*, 2023, **629**, 157454.
18 C.-W. Pai and G.-S. Wang, *Chemosphere*, 2022, **287**, 132171.
19 S. Kumar, R. S. Brar, J. N. Babu and K. Hussain, in *Industrial Applications*, ed. R. S. Varma and B. Banerjee, De Gruyter, 2022, pp. 1–36.
20 S. Kumar, P. Kaur, R. S. Brar and J. N. Babu, *Heliyon*, 2022, **8**, e10140.
21 T. Liu, C. O. Aniagor, M. I. Ejimofor, M. C. Menkiti, K. H. D. Tang, B. L. F. Chin, Y. H. Chan, C. L. Yiin, K. W. Cheah, Y. Ho Chai, S. S. M. Lock, K. L. Yap, M. X. J. Wee and P.-S. Yap, *J. Mol. Liq.*, 2023, **374**, 121144.
22 Y. Li, X. Wang, Z. Li, M. Chen, J. Zheng and X. Wang, *Chem. Eng. J.*, 2023, **475**, 146036.
23 R. Liang, R. Huang, S. Ying, X. Wang, G. Yan and L. Wu, *Nano Res.*, 2018, **11**, 1109–1123.
24 K. Sharma, S. Kaushal, A. Jain, M. H. Sami, S. Kumar, H. Tariq, K. Bano, S. Aggarwal, R. Kumar and P. P. Singh, *Chem. Pap.*, 2024, **78**, 2757–2782.
25 N. G. Dlamini, A. K. Basson and V. S. R. Pullabhotla, *Appl. Nano*, 2023, **4**, 1–24.
26 K. Loza, M. Heggen and M. Epple, *Adv. Funct. Mater.*, 2020, **30**, 1909260.
27 N. Arora, K. Thangavelu and G. N. Karanikolos, *Front. Chem.*, 2020, **8**, 412.
28 M. Duan, L. Jiang, G. Zeng, D. Wang, W. Tang, J. Liang, H. Wang, D. He, Z. Liu and L. Tang, *Appl. Mater. Today*, 2020, **19**, 100564.

29 D. Medina-Cruz, B. Saleh, A. Vernet-Crua, A. Nieto-Argüello, D. Lomelí-Marroquín, L. Y. Vélez-Escamilla, J. L. Cholula-Díaz, J. M. García-Martín and T. Webster, in *Racing for the Surface*, ed. B. Li, T. F. Moriarty, T. Webster and M. Xing, Springer International Publishing, Cham, 2020, pp. 397–434.
30 Y.-H. Li, J.-Y. Li and Y.-J. Xu, *EnergyChem*, 2021, **3**, 100047.
31 L. Liu and A. Corma, *Chem. Rev.*, 2023, **123**, 4855–4933.
32 R. Wei, N. Tang, L. Jiang, J. Yang, J. Guo, X. Yuan, J. Liang, Y. Zhu, Z. Wu and H. Li, *Coord. Chem. Rev.*, 2022, **462**, 214500.
33 A. Kaur, G. Kaur, P. P. Singh and S. Kaushal, *Int. J. Hydrog. Energy*, 2021, **46**, 15820–15849.
34 S. Bharti, *World J. Microbiol. Biotechnol.*, 2024, **40**, 89.
35 O. T. Fanoro and O. S. Oluwafemi, *Pharmaceutics*, 2020, **12**, 1044.
36 R. Stephanie, M. W. Kim, S. H. Kim, J.-K. Kim, C. Y. Park and T. J. Park, *Trac. Trends Anal. Chem.*, 2021, **135**, 116159.
37 J. Scaria, P. V. Nidheesh and M. S. Kumar, *J. Environ. Manage.*, 2020, **259**, 110011.
38 R. Rajeev, R. Datta, A. Varghese, Y. N. Sudhakar and L. George, *Microchem. J.*, 2021, **163**, 105910.
39 C. Singh, A. K. Mehata, V. Priya, A. K. Malik, A. Setia, M. N. L. Suseela, P. Gokul, S. K. Singh and M. S. Muthu, *Molecules*, 2022, **27**, 7059.
40 M. D. Makhafola, S. A. Balogun and K. D. Modibane, *Energies*, 2024, **17**, 1646.
41 Z. Swiatkowska-Warkocka, *Appl. Sci.*, 2021, **11**, 1978.
42 K. G. N. Quiton, M.-C. Lu and Y.-H. Huang, *Chemosphere*, 2021, **262**, 128371.
43 A. Nyabadza, É. McCarthy, M. Makhesana, S. Heidarinassab, A. Plouze, M. Vazquez and D. Brabazon, *Adv. Colloid Interface Sci.*, 2023, **321**, 103010.
44 D. S. Idris and A. Roy, *Crystals*, 2023, **13**, 637.
45 B. K. Allam, N. Musa, A. Debnath, U. L. Usman and S. Banerjee, *Environ. Chall.*, 2021, **5**, 100405.
46 G. A. Kifle, Y. Huang, M. Xiang, W. Wang, C. Wang, C. Li and H. Li, *Chem. Eng. J.*, 2022, **442**, 136187.
47 A. A. Aryee, Y. Liu, R. Han and L. Qu, *Environ. Chem. Lett.*, 2023, **21**, 1811–1835.
48 M. Larrañaga-Tapia, B. Betancourt-Tovar, M. Videa, M. Antunes-Ricardo and J. L. Cholula-Díaz, *Nanoscale Adv.*, 2024, **6**, 51–71.
49 A. Saravanan, P. S. Kumar, S. Karishma, D.-V. N. Vo, S. Jeevanantham, P. R. Yaashikaa and C. S. George, *Chemosphere*, 2021, **264**, 128580.
50 A. Scala, G. Neri, N. Micale, M. Cordaro and A. Piperno, *Molecules*, 2022, **27**, 1134.
51 J. De Bellis, M. Felderhoff and F. Schüth, *Chem. Mater.*, 2021, **33**, 2037–2045.
52 H. Chen, C. Wang, M. Zheng, C. Liu, W. Li, Q. Yang, S. Zhou and X. Feng, *J. Energy Chem.*, 2023, **84**, 210–218.
53 F. Xu, S. Deng, J. Xu, W. Zhang, M. Wu, B. Wang, J. Huang and G. Yu, *Environ. Sci. Technol.*, 2012, **46**, 4576–4582.
54 V. Amendola and M. Meneghetti, *Phys. Chem. Chem. Phys.*, 2013, **15**, 3027–3046.
55 D. Zhang, B. Gökce, C. Notthoff and S. Barcikowski, *Sci. Rep.*, 2015, **5**, 13661.
56 J. L. H. Chau, C.-Y. Chen, M.-C. Yang, K.-L. Lin, S. Sato, T. Nakamura, C.-C. Yang and C.-W. Cheng, *Mater. Lett.*, 2011, **65**, 804–807.
57 M. Blosi, S. Ortelli, A. Costa, M. Dondi, A. Lolli, S. Andreoli, P. Benito and S. Albonetti, *Materials*, 2016, **9**, 550.
58 F. Ameen, R. N. E. Tiri, M. Bekmezci, F. Karimi, N. Bennini and F. Sen, *Chemosphere*, 2023, **339**, 139630.
59 P. N. Njoki, A. E. Rhoades and J. I. Barnes, *Mater. Chem. Phys.*, 2020, **241**, 122348.
60 A. V. Pervikov, S. O. Kazantsev, A. S. Lozhkomoev and M. I. Lerner, *Powder Technol.*, 2020, **372**, 136–147.
61 F. Zhan, J. Yin, A. Zhang, J. Zhou, M. Wang and T. Jiao, *Appl. Surf. Sci.*, 2020, **527**, 146719.
62 Y. He, H. Lin, Y. Dong, B. Li, L. Wang, S. Chu, M. Luo and J. Liu, *Chem. Eng. J.*, 2018, **347**, 669–681.
63 S. Anandan, F. Grieser and M. Ashokkumar, *J. Phys. Chem. C*, 2008, **112**, 15102–15105.
64 R. Mirzajani and S. Karimi, *Ultrason. Sonochem.*, 2019, **50**, 239–250.
65 C. Kan, W. Cai, C. Li, L. Zhang and H. Hofmeister, *J. Phys. Appl. Phys.*, 2003, **36**, 1609–1614.
66 T. Redjala, H. Remita, G. Apostolescu, M. Mostafavi, C. Thomazeau and D. Uzio, *Oil Gas Sci. Technol.*, 2006, **61**, 789–797.
67 S. Kianfar, A. N. Golikand and B. ZareNezhad, *J. Nanostructure Chem.*, 2021, **11**, 287–299.
68 M. Treguer, C. De Cointet, H. Remita, J. Khatouri, M. Mostafavi, J. Amblard, J. Belloni and R. De Keyzer, *J. Phys. Chem. B*, 1998, **102**, 4310–4321.
69 H. Eslami, M. H. Ehrampoush, A. Esmaeili, A. A. Ebrahimi, M. T. Ghaneian, H. Falahzadeh and M. H. Salmani, *Mater. Chem. Phys.*, 2019, **224**, 65–72.
70 U. Lawal Usman, B. Kumar Allam, N. Bahadur Singh and S. Banerjee, *J. Mol. Liq.*, 2022, **354**, 118833.
71 F. Gao, C. Yang, X. Tang, H. Yi and C. Wang, *Environ. Sci. Pollut. Res.*, 2022, **29**, 21210–21220.
72 L. Chen, B.-Y. He, S. He, T.-J. Wang, C.-L. Su and Y. Jin, *Powder Technol.*, 2012, **227**, 3–8.
73 Y. Absalan, M. A. Ryabov and O. V. Kovalchukova, *Mater. Sci. Eng. C*, 2019, **97**, 813–826.
74 T. I. Asanova, I. P. Asanov, M.-G. Kim, E. Yu. Gerasimov, A. V. Zadesenets, P. E. Plyusnin and S. V. Korenev, *J. Nanoparticle Res.*, 2013, **15**, 1994.
75 K. Ding, L. Liu, Y. Cao, X. Yan, H. Wei and Z. Guo, *Int. J. Hydrog. Energy*, 2014, **39**, 7326–7337.
76 L.-M. Luo, R.-H. Zhang, D. Chen, Q.-Y. Hu, X. Zhang, C.-Y. Yang and X.-W. Zhou, *Electrochim. Acta*, 2018, **259**, 284–292.
77 O. V. Belousov, N. V. Belousova, A. V. Sirotina, L. A. Solovyov, A. M. Zhyzhaev, S. M. Zharkov and Y. L. Mikhlin, *Langmuir*, 2011, **27**, 11697–11703.
78 H. Goksu, M. Bekmezci, R. Bayat, E. E. Altuner and F. Şen, in *Nanomaterials for Direct Alcohol Fuel Cells*, Elsevier, 2021, pp. 433–447.

79 E. L. De León-Quiroz, D. V. Obregón, A. P. Pedraza, E. Larios-Rodríguez, M. José-Yacaman and L. A. García-Cerda, *MRS Proc.*, 2012, **1479**, 9–14.
80 F. Jiang, G. Feng, C. Xu, S. Qing, Q. Wu, Y. Yu, Q. Zhang and W. Jiang, *J. Sol-Gel Sci. Technol.*, 2021, **100**, 555–561.
81 N. N. Gubanova, V. A. Matveev and O. A. Shilova, *J. Sol-Gel Sci. Technol.*, 2019, **92**, 367–375.
82 M. A. Malik, M. Y. Wani and M. A. Hashim, *Arab. J. Chem.*, 2012, **5**, 397–417.
83 J. Lu, Z. Wen, Y. Zhang, G. Cheng, R. Xu, X. Gong, X. Wang and R. Chen, *Sci. Total Environ.*, 2021, **762**, 143163.
84 J. Wu, M. Lin, X. Weng, G. Owens and Z. Chen, *Chem. Eng. J.*, 2021, **408**, 127273.
85 F. T. Quinlan, J. Kuther, W. Tremel, W. Knoll, S. Risbud and P. Stroeve, *Langmuir*, 2000, **16**, 4049–4051.
86 T. Szumełda, A. Drelinkiewicz, R. Kosydar, J. Gurgul and D. Duraczyńska, *J. Mater. Sci.*, 2021, **56**, 392–414.
87 G. Sharma, A. Kumar, S. Sharma, Mu. Naushad, R. Prakash Dwivedi, Z. A. ALOthman and G. T. Mola, *J. King Saud Univ.-Sci.*, 2019, **31**, 257–269.
88 Y. Wang, P. Zhang, X. Mao, W. Fu and C. Liu, *Sens. Actuators, B*, 2016, **231**, 95–101.
89 L. Chen, A. Leonardi, J. Chen, M. Cao, N. Li, D. Su, Q. Zhang, M. Engel and X. Ye, *Nat. Commun.*, 2020, **11**, 3041.
90 G.-H. Han, K. Y. Kim, H. Nam, H. Kim, J. Yoon, J.-H. Lee, H.-K. Kim, J.-P. Ahn, S. Y. Lee, K.-Y. Lee and T. Yu, *Catalysts*, 2020, **10**, 650.
91 S. S. Emmanuel, A. A. Adesibikan, O. D. Saliu and E. A. Opatola, *Plant Nano Biol.*, 2023, **3**, 100024.
92 L. Berta, N.-A. Coman, A. Rusu and C. Tanase, *Materials*, 2021, **14**, 7677.
93 K. S. Sasireka and P. Lalitha, *Rev. Inorg. Chem.*, 2021, **41**, 223–244.
94 Y. Tuo, G. Liu, B. Dong, H. Yu, J. Zhou, J. Wang and R. Jin, *Environ. Sci. Pollut. Res.*, 2017, **24**, 5249–5258.
95 R. Han, X. Song, Q. Wang, Y. Qi, G. Deng, A. Zhang, Q. Wang, F. Chang, C. Wu and Y. Cheng, *J. Chem. Technol. Biotechnol.*, 2019, **94**, 3375–3383.
96 J. Liu, Y. Zheng, Z. Hong, K. Cai, F. Zhao and H. Han, *Sci. Adv.*, 2016, **2**, e1600858.
97 X. Jiang, X. Fan, W. Xu, R. Zhang and G. Wu, *ACS Biomater. Sci. Eng.*, 2020, **6**, 680–689.
98 K. Deplanche, M. L. Merroun, M. Casadesus, D. T. Tran, I. P. Mikheenko, J. A. Bennett, J. Zhu, I. P. Jones, G. A. Attard, J. Wood, S. Selenska-Pobell and L. E. Macaskie, *J. R. Soc. Interface*, 2012, **9**, 1705–1712.
99 J. Gomez-Bolivar, I. P. Mikheenko, R. L. Orozco, S. Sharma, D. Banerjee, M. Walker, R. A. Hand, M. L. Merroun and L. E. Macaskie, *Front. Microbiol.*, 2019, **10**, 1276.
100 F. Ameen, *Appl. Sci.*, 2022, **12**, 1384.
101 M. Ovais, A. Khalil, M. Ayaz, I. Ahmad, S. Nethi and S. Mukherjee, *Int. J. Mol. Sci.*, 2018, **19**, 4100.
102 N. A. N. Mohamad, J. Jai, N. A. Arham and A. Hadi, in *2013 IEEE International Conference on Control System, Computing and Engineering*, IEEE, Penang, Malaysia, 2013, pp. 334–339.
103 J. A. Hernández-Díaz, J. J. Garza-García, A. Zamudio-Ojeda, J. M. León-Morales, J. C. López-Velázquez and S. García-Morales, *J. Sci. Food Agric.*, 2021, **101**, 1270–1287.
104 A. Lateef, S. A. Ojo, B. I. Folarin, E. B. Gueguim-Kana and L. S. Beukes, *J. Clust. Sci.*, 2016, **27**, 1561–1577.
105 B. A. Providence, A. A. Chinyere, A. A. Ayi, O. O. Charles, T. A. Elijah and H. L. Ayomide, *Int. J. Phys. Sci.*, 2018, **13**, 24–32.
106 C. Prasad, K. Sreenivasulu, S. Gangadhara and P. Venkateswarlu, *J. Alloys Compd.*, 2017, **700**, 252–258.
107 S. Mondal, N. Roy, R. A. Laskar, I. Sk, S. Basu, D. Mandal and N. A. Begum, *Colloids Surf. B Biointerfaces*, 2011, **82**, 497–504.
108 S. S. Shankar, A. Rai, A. Ahmad and M. Sastry, *J. Colloid Interface Sci.*, 2004, **275**, 496–502.
109 D. S. Sheny, J. Mathew and D. Philip, *Spectrochim. Acta, Part A*, 2011, **79**, 254–262.
110 J. Al-Haddad, F. Alzaabi, P. Pal, K. Rambabu and F. Banat, *Clean Technol. Environ. Policy*, 2020, **22**, 269–277.
111 G. Mamatha, A. Varada Rajulu and K. Madhukar, *J. Nat. Fibers*, 2020, **17**, 1121–1129.
112 D. Alti, M. Veeramohan Rao, D. N. Rao, R. Maurya and S. K. Kalangi, *ACS Omega*, 2020, **5**, 16238–16245.
113 M. Meena Kumari, J. Jacob and D. Philip, *Spectrochim. Acta, Part A*, 2015, **137**, 185–192.
114 B. S. Sivamaruthi, V. S. Ramkumar, G. Archunan, C. Chaiyasut and N. Suganthy, *J. Drug Deliv. Sci. Technol.*, 2019, **51**, 139–151.
115 S. Velpula, S. R. Beedu and K. Rupula, *Int. J. Biol. Macromol.*, 2021, **190**, 159–169.
116 U. Younas, S. Hassan, F. Ali, F. Hassan, Z. Saeed, M. Pervaiz, S. Khan, F. Jannat, S. Bibi, A. Sadiqa, Z. Ali, S. Iqbal, A. Ghfar, M. Ouladsmane, M. AL-Anazy and S. Ali, *Coatings*, 2021, **11**, 813.
117 B. Akilandaeaswari and K. Muthu, *J. Taiwan Inst. Chem. Eng.*, 2021, **127**, 292–301.
118 C. Tamuly, M. Hazarika, S. Ch. Borah, M. R. Das and M. P. Boruah, *Colloids Surf. B Biointerfaces*, 2013, **102**, 627–634.
119 F. Gulbagça, A. Aygun, E. E. Altuner, M. Bekmezci, T. Gur, F. Sen, H. Karimi-Maleh, N. Zare, F. Karimi and Y. Vasseghian, *Chem. Eng. Res. Des.*, 2022, **180**, 254–264.
120 Z. Terzopoulou, A. Zamboulis, I. Koumentakou, G. Michailidou, M. J. Noordam and D. N. Bikiaris, *Biomacromolecules*, 2022, **23**, 1841–1863.
121 K. Sharma, H. Singh, G. Singh, N. Kaur, P. Kumar Pati, K. Singh, A. Kumar and T. S. Kang, *Nanoscale*, 2024, **16**, 17549–17558.
122 T. Aydemir, G. Dzhardimalieva, E. Kasymova, L. Rabinskiy, O. Tushavina and K. Kydralieva, *Mater. Today Proc.*, 2021, **34**, 322–325.
123 A. K. Sharma, P. Mehara and P. Das, *ACS Catal.*, 2022, **12**, 6672–6701.
124 S. Pedroso-Santana and N. Fleitas-Salazar, *Part. Part. Syst. Charact.*, 2023, **40**, 2200146.
125 S. Ashraf, Y. Liu, H. Wei, R. Shen, H. Zhang, X. Wu, S. Mehdi, T. Liu and B. Li, *Small*, 2023, **19**, 2303031.

126 H. Zhang, L. Wang, L. Lu and N. Toshima, *Sci. Rep.*, 2016, **6**, 30752.
127 J. Wang, C. Liu, I. Hussain, C. Li, J. Li, X. Sun, J. Shen, W. Han and L. Wang, *RSC Adv.*, 2016, **6**, 54623–54635.
128 J. Liu, Z. Wu, Q. He, Q. Tian, W. Wu, X. Xiao and C. Jiang, *Nanoscale Res. Lett.*, 2019, **14**, 35.
129 K. C. Pingali, S. Deng and D. A. Rockstraw, *Chem. Eng. Commun.*, 2007, **194**, 780–786.
130 Y. Ding, F. Fan, Z. Tian and Z. L. Wang, *J. Am. Chem. Soc.*, 2010, **132**, 12480–12486.
131 K. Shim, J. Lin, M.-S. Park, M. Shahabuddin, Y. Yamauchi, M. S. A. Hossain and J. H. Kim, *Scr. Mater.*, 2019, **158**, 38–41.
132 J. Sopoušek, J. Pinkas, P. Brož, J. Buršík, V. Vykoukal, D. Škoda, A. Stýskalík, O. Zobač, J. Vřeštál, A. Hrdlička and J. Šimbera, *J. Nanomater.*, 2014, **2014**, 1–13.
133 B. W. Boote, H. Byun and J.-H. Kim, *Gold Bull.*, 2013, **46**, 185–193.
134 A. Wilson, R. Bernard, A. Vlad, Y. Borensztein, A. Coati, B. Croset, Y. Garreau and G. Prévot, *Phys. Rev. B*, 2014, **90**, 075416.
135 A. L. Querejeta, M. C. Del Barrio and S. G. García, *J. Electroanal. Chem.*, 2016, **778**, 98–102.
136 M. Oezaslan, F. Hasché and P. Strasser, *Chem. Mater.*, 2011, **23**, 2159–2165.
137 E. E. Elemike, D. C. Onwudiwe, N. Nundkumar, M. Singh and O. Iyekowa, *Mater. Lett.*, 2019, **243**, 148–152.
138 T. A. Saleh, *J. Clean. Prod.*, 2018, **172**, 2123–2132.
139 D. Raju, R. Mendapara and U. J. Mehta, *Mater. Lett.*, 2014, **124**, 271–274.
140 I. Auwal, B. Ünal, A. Baykal, U. Kurtan and A. Yıldız, *J. Supercond. Nov. Magn.*, 2017, **30**, 1499–1514.
141 N. Moghimi, M. Mohapatra and K. T. Leung, *Anal. Chem.*, 2015, **87**, 5546–5552.
142 P. Srinoi, Y.-T. Chen, V. Vittur, M. D. Marquez and T. R. Lee, *Appl. Sci.*, 2018, **8**, 1106.
143 A. Mirzaei, K. Janghorban, B. Hashemi, M. Bonyani, S. G. Leonardi and G. Neri, *J. Nanostructure Chem.*, 2017, **7**, 37–46.
144 T. V. Tsoulos, L. Han, J. Weir, H. L. Xin and L. Fabris, *Nanoscale*, 2017, **9**, 3766–3773.
145 Y. Jia, H. Niu, M. Wu, M. Ning, H. Zhu and Q. Chen, *Mater. Res. Bull.*, 2005, **40**, 1623–1629.
146 L. F. F. P. G. Bragança, R. R. Avilez and M. I. P. D. Silva, *Colloids Surf. A Physicochem. Eng. Asp.*, 2010, **358**, 79–87.
147 M. Ragothaman, B. T. Mekonnen and T. Palanisamy, *Mater. Chem. Phys.*, 2020, **253**, 123405.
148 N. Bhattarai, S. Khanal, D. Bahena, R. L. Whetten and M. Jose-Yacaman, *MRS Proc.*, 2014, **1708**, 59–91.
149 L. Yu, L. He, J. Chen, J. Zheng, L. Ye, H. Lin and Y. Yuan, *ChemCatChem*, 2015, **7**, 1701–1707.
150 O. Ahumada, M. M. Pérez-Madrigal, J. Ramirez, D. Curcó, C. Esteves, A. Salvador-Matar, G. Luongo, E. Armelin, J. Puiggalí and C. Alemán, *Rev. Sci. Instrum.*, 2013, **84**, 053904.
151 E. A. Koroleva, I. D. Shabalkin and P. V. Krivoshapkin, *J. Mater. Chem. B*, 2023, **11**, 3054–3070.
152 A. Nyabadza, É. McCarthy, M. Makhesana, S. Heidarinassab, A. Plouze, M. Vazquez and D. Brabazon, *Adv. Colloid Interface Sci.*, 2023, **321**, 103010.
153 B.-Y. Wen, Q.-Q. Chen, P. M. Radjenovic, J.-C. Dong, Z.-Q. Tian and J.-F. Li, *Annu. Rev. Phys. Chem.*, 2021, **72**, 331–351.
154 G. Lama, J. Meijide, A. Sanromán and M. Pazos, *Catalysts*, 2022, **12**, 344.
155 M. A. Tahoon, S. M. Siddeeg, N. Salem Alsaiari, W. Mnif and F. Ben Rebah, *Processes*, 2020, **8**, 645.
156 E. C. Foo, M. Russell, O. Lily and H. L. Ford, *Mult. Scler. Relat. Disord.*, 2020, **44**, 102330.
157 Q. Xu, H. Fu, J. Gu, L. Lei and L. Ling, *J. Environ. Sci.*, 2025, **148**, 614–624.
158 K. Świacka, A. Michnowska, J. Maculewicz, M. Caban and K. Smolarz, *Environ. Pollut.*, 2021, **273**, 115891.
159 V. Rout, B. Barik, D. K. Panda, S. Subudhi, A. Mohapatra, R. K. Sharma and P. Dash, *Ind. Eng. Chem. Res.*, 2024, **63**, 8054–8075.
160 H. M. Abdel-Aziz, R. S. Farag and S. A. Abdel-Gawad, *J. Environ. Eng. Sci.*, 2020, **15**, 119–129.
161 D. Vasu, A. K. Keyan, P. Moorthi, S. Sakthinathan, C.-L. Yu and T.-W. Chiu, *J. Environ. Chem. Eng.*, 2023, **11**, 109055.
162 A. A. Gonçalves, A. F. Araújo, J. P. De Mesquita, M. J. M. Pires, R. M. Verly, L. M. Da Silva and D. V. Franco, *J. Environ. Chem. Eng.*, 2016, **4**, 4354–4365.
163 A. F. Araújo, A. A. Gonçalves, F. G. L. Rosado, R. M. Verly, L. M. Da Silva and D. V. Franco, *Clean: Soil, Air, Water*, 2017, **45**, clen.201500977.
164 P. E. Ohale, C. A. Igwegbe, K. O. Iwuozor, E. C. Emenike, C. C. Obi and A. Białowiec, *MethodsX*, 2023, **10**, 102180.
165 Y. Du, Z. Li, R. Feng, Q. Liu, Y. Yang, M. Sun, Y. Zhao, T. Yan and L. Yan, *J. Environ. Chem. Eng.*, 2024, **12**, 112324.
166 H. Wang, X. Zhang, Y. Wang, G. Quan, X. Han and J. Yan, *Nanomaterials*, 2018, **8**, 664.
167 S. J. Mohammed, M. J. M-Ridha, K. M. Abed and A. A. M. Elgharbawy, *Int. J. Environ. Anal. Chem.*, 2023, **103**, 3801–3819.
168 I. A. Ahmed, H. S. Hussein, Z. A. ALOthman, A. G. ALanazi, N. S. Alsaiari and A. Khalid, *Polymers*, 2023, **15**, 1221.
169 L. Chen, T. Yuan, R. Ni, Q. Yue and B. Gao, *Chem. Eng. J.*, 2019, **365**, 183–192.
170 N. B. Karunarathna, I. A. Perera, N. T. Nayomi, D. M. S. Munasinghe, S. S. P. Silva, I. Strashnov, B. R. Fernando and J. Natl, *Sci. Found. Sri Lanka*, 2021, **49**, 479.
171 M.-Y. Ibrahim Mohamed, *Nutr. Food Sci. Int. J.*, 2021, **11**(1), 555801.
172 L. Yu, Y. Zhao, S. Guo and J. Xue, *Catal. Lett.*, 2024, **154**(9), 5255–5269.
173 C. Zheng, C. Yang, X. Cheng, S. Xu, Z. Fan, G. Wang, S. Wang, X. Guan and X. Sun, *Sep. Purif. Technol.*, 2017, **189**, 357–365.
174 A. Angeli, in *Metalloenzymes*, Elsevier, 2024, pp. 23–34.
175 D. Ayodhya, V. Sumalatha, R. Gurrapu and M. Sharath Babu, *Results Chem.*, 2023, **5**, 100792.

176 V. Queirós, U. M. Azeiteiro, A. M. V. M. Soares and R. Freitas, *J. Hazard. Mater.*, 2021, **412**, 125028.
177 L. T. Pérez-Poyatos, L. M. Pastrana-Martínez, S. Morales-Torres, P. Sánchez-Moreno, M. Bramini and F. J. Maldonado-Hódar, *Catal. Today*, 2023, **423**, 114010.
178 L. Qiu, C. Yan, Y. Zhang, Y. Chen and M. Nie, *Environ. Pollut.*, 2024, **350**, 124039.
179 L. Niu, X. Zhao, Z. Tang, Y. Cai, Q. Lei, D. Hou, H. Niu, L. Wang, J. P. Giesy and F. Wu, *Sci. Total Environ.*, 2023, **892**, 164587.
180 M. SefidSiahbandi, O. Moradi, B. Akbari –Adergani, P. A. Azar and M. S. Tehrani, *Chemosphere*, 2023, **312**, 137184.
181 S. Kaushal, P. Pal Singh and N. Kaur, *Environ. Nanotechnol. Monit. Manag.*, 2022, **18**, 100727.
182 M. Musa, H. Hasan, H. Malkoç, M. Ergüt, D. Uzunoğlu and A. Özer, *Turk. J. Eng.*, 2020, **4**, 209–217.
183 G. Gopal, H. Sankar, C. Natarajan and A. Mukherjee, *J. Environ. Manage.*, 2020, **254**, 109812.
184 C. O. Aniagor, C. A. Igwegbe, J. O. Ighalo and S. N. Oba, *J. Mol. Liq.*, 2021, **334**, 116124.
185 M. SefidSiahbandi, O. Moradi, B. Akbari-adergani, P. Aberoomand Azar and M. Sabar Tehrani, *Environ. Res.*, 2023, **218**, 114925.
186 W. Qiu, B. Chen, L. Tang, C. Zheng, B. Xu, Z. Liu, J. T. Magnuson, S. Zhang, D. Schlenk, E. G. Xu and B. Xing, *Environ. Sci. Technol.*, 2022, **56**, 4251–4261.
187 S. Xia, J. Sun and W. Sun, *Colloids Surf. A Physicochem. Eng. Asp.*, 2022, **649**, 129403.
188 M. Sharma, *Asian J. Pharm. Clin. Res.*, 2021, 64–68.
189 X. Jin, H. Li, X. Zhu, N. Li, G. Owens and Z. Chen, *J. Environ. Manage.*, 2022, **318**, 115526.
190 C. H. Nguyen, M. L. Tran, T. T. Van Tran and R.-S. Juang, *J. Taiwan Inst. Chem. Eng.*, 2021, **119**, 80–89.
191 R. Zuo, X. Liu, Q. Zhang, J. Wang, J. Yang, Y. Teng, X. Chen and Y. Zhai, *Ecol. Eng.*, 2021, **162**, 106175.
192 Q. Dong, H. Dong, Y. Li, J. Xiao, S. Xiang, X. Hou and D. Chu, *J. Hazard. Mater.*, 2022, **431**, 128601.
193 L. M. Mahlaule-Glory, S. Mathobela and N. C. Hintsho-Mbita, *Catalysts*, 2022, **12**, 334.
194 M. Parolini, *Sci. Total Environ.*, 2020, **740**, 140043.
195 M. Şahin, Y. Arslan and F. Tomul, *Res. Chem. Intermed.*, 2022, **48**, 5209–5226.
196 L. He, L. Lv, S. C. Pillai, H. Wang, J. Xue, Y. Ma, Y. Liu, Y. Chen, L. Wu, Z. Zhang and L. Yang, *Sci. Total Environ.*, 2021, **783**, 146974.
197 A. Ghauch, H. Abou Assi and S. Bdeir, *J. Hazard. Mater.*, 2010, **182**, 64–74.
198 Y. Pan, Q. Ding, B. Li, X. Wang, Y. Liu, J. Chen, F. Ke and J. Liu, *Chemosphere*, 2021, **263**, 128101.
199 K. K. Sodhi, M. Kumar and D. K. Singh, *J. Water Process Eng.*, 2021, **39**, 101858.
200 J. Wen, X. Liu, L. Liu, X. Ma, A. Fakhri and V. K. Gupta, *Colloids Surf. A Physicochem. Eng. Asp.*, 2021, **610**, 125683.
201 Y. Zhang, B.-T. Zhang, Y. Teng, J. Zhao, L. Kuang and X. Sun, *J. Hazard. Mater.*, 2020, **400**, 123290.
202 A. R. Yazdanbakhsh, H. Daraei, M. Rafiee and H. Kamali, *Water Sci. Technol.*, 2016, **73**, 2998–3007.
203 A. Parrella, M. Lavorgna, E. Criscuolo, C. Russo, V. Fiumano and M. Isidori, *Chemosphere*, 2014, **115**, 59–66.
204 H. Fu, R. Wang, Q. Xu, M. Laipan, C. Tang, W. Zhang and L. Ling, *Appl. Catal. B Environ.*, 2021, **299**, 120686.
205 B. S. Kadu, K. D. Wani, R. Kaul-Ghanekar and R. C. Chikate, *Chem. Eng. J.*, 2017, **325**, 715–724.
206 E. P. Ambrosio-Albuquerque, L. F. Cusioli, R. Bergamasco, A. A. Sinópolis Gigliolli, L. Lupepsa, B. R. Paupitz, P. A. Barbieri, L. A. Borin-Carvalho and A. L. De Brito Portela-Castro, *Environ. Toxicol. Pharmacol.*, 2021, **83**, 103588.
207 H. M. Abd El-Aziz, R. S. Farag and S. A. Abdel-Gawad, *Nanotechnol. Environ. Eng.*, 2020, **5**, 23.
208 S. Campos, R. Salazar, N. Arancibia-Miranda, M. A. Rubio, M. Aranda, A. García, P. Sepúlveda and L. C. Espinoza, *Chemosphere*, 2020, **247**, 125813.
209 H. M. Abdel-Aziz, R. S. Farag and S. A. Abdel-Gawad, *Int. J. Environ. Res.*, 2019, **13**, 843–852.
210 S. Kumar, T. Paul, S. P. Shukla, K. Kumar, S. Karmakar, K. K. Bera and C. Bhushan Kumar, *Environ. Pollut.*, 2021, **286**, 117569.
211 Y. Lin, X. Jin, G. Owens and Z. Chen, *Sci. Total Environ.*, 2019, **695**, 133878.
212 J.-F. Gao, Z.-L. Wu, W.-J. Duan and W.-Z. Zhang, *Sci. Total Environ.*, 2019, **662**, 978–989.
213 S. Xia, J. Sun and W. Sun, *Colloids Surf. A Physicochem. Eng. Asp.*, 2022, **649**, 129403.
214 L. He, L. Lv, S. C. Pillai, H. Wang, J. Xue, Y. Ma, Y. Liu, Y. Chen, L. Wu, Z. Zhang and L. Yang, *Sci. Total Environ.*, 2021, **783**, 146974.